SETD3 is an Actin Histidine Methyltransferase that Prevents Primary Dystocia

Alex W. Wilkinson[1,*], **Jonathan Diep**[2,*], **Shaobo Dai**[3,*], **Shuo Liu**[1], **Yaw shin Ooi**[2], **Dan Song**[4], **Tie-Mei Li**[1], **John R. Horton**[3], **Xing Zhang**[3], **Chao Liu**[4], **Darshan V. Trivedi**[4], **Katherine M. Ruppel**[4], **José G. Vilches-Moure**[5], **Kerriann M. Casey**[5], **Justin Mak**[6], **Tina Cowan**[7], **Joshua E. Elias**[8], **Claude M. Nagamine**[5], **James A. Spudich**[4], **Xiaodong Cheng**[3,#], **Jan E. Carette**[2,#], **Or Gozani**[1,#]

[1]Department of Biology, Stanford University, Stanford, CA 94305, USA

[2]Department of Microbiology and Immunology, Stanford University School of Medicine, Stanford, CA 94305, USA

[3]Department of Molecular and Cellular Oncology, The University of Texas MD Anderson Cancer Center, Houston, TX 77030, USA

[4]Department of Biochemistry, Stanford University School of Medicine, Stanford, CA 94305, USA

[5]Department of Comparative Medicine, Stanford University School of Medicine, Stanford, CA 94305, USA

[6]Stanford Healthcare, Palo Alto, CA 94305 USA

[7]Deparient of Pathology, Stanford University School of Medicine, Stanford, CA 94305, USA

[8]Deparment of Chemical and Systems Biology, Stanford University School of Medicine, Stanford CA 94305, USA

Abstract

For over fifty years, the methylation of mammalian actin at histidine 73 (actin-H73me) has been known to exist[1]. Beyond mammals, we find that actin-H73me is conserved in several additional model animal and plant organisms. Despite the pervasiveness of H73me, its function is enigmatic, and the enzyme generating this modification is unknown. Here, we identify SETD3 (SET domain protein 3) as the physiologic actin histidine 73 methyltransferase. Structural studies

[#]To whom correspondence should be addressed: ogozani@stanford.edu; carette@stanford.edu; xcheng5@mdanderson.org.
[*]These authors contributed equally to the work

reveal that an extensive network of interactions clamps the actin peptide on the SETD3 surface to properly orient H73 within the catalytic pocket and facilitate methyl transfer. H73me reduces the nucleotide exchange rate on actin monomers and modestly accelerates actin filament assembly. Mice lacking SETD3 show complete loss of actin-H73me in multiple tissues and quantitative proteomics singles out actin-H73 as the principal physiologic SETD3 substrate. SETD3 deficient female mice have severely decreased litter sizes due to primary maternal dystocia that is refractory to ecbolic induction agents. Further, depletion of SETD3 impairs signal-induced contraction in primary human uterine smooth muscle cells. Together, our results identify the first mammalian protein histidine methyltransferase and uncover a pivotal role for SETD3 and actin-H73me in the regulation of smooth muscle contractility. Our data also support the broader hypothesis where protein histidine methylation acts as a common regulatory mechanism.

SETD3, a ubiquitously expressed protein, is epigenetically up-regulated in response to muscle loading and hypertrophy[2]. SETD3 contains an N-terminal SET domain and a C-terminal domain homologous to a Rubisco large subunit methyltransferase (LSMT) interaction domain (Extended Data Fig. 1a). Proteins containing the catalytic lysine methyltransferase SET domain are found in all three kingdoms of life and regulate diverse biological and pathologic processes[3]. In humans, ~half of the fifty-five SET family members methylate lysines on histone and/or non-histone protein substrates[3]. Enzymatic activities for the remainder of human SET proteins, including SETD3, are unclear. SETD3 was reported to methylate histone H3 at lysines 4 and 36[4]. However, this conclusion was based on mass spectrometry data wherin mass shifts were inconsistent with a bona fide methylation event (see Figure 2C in[4]). When we tested SETD3 activity, it did not methylate histones in contrast to two established protein lysine methyltransferases (PKMTs), NSD2 and MLL2[3] (Fig. 1a and Extended Data Fig. 1b). Based on these results and the cytoplasmic localization of SETD3 (Extended Data Fig. 1c), we conclude that SETD3 is not a histone methyltransferase and likely targets a non-histone substrate.

Among active PKMTs, SETD3 is most similar to human SETD6[5]. We generated a putative SETD3 catalytic mutant based on this homology (Extended Data Fig. 1a) and performed *in vitro* methylation assays with ^{3}H-SAM (*S*-adenosyl-methionine) on total cytoplasmic extract with wild-type or mutant SETD3. A ~42 kDa band was more prominent in reactions with wild-type SETD3 relative to the mutant (Fig. 1b). A three-step fractionation protocol was used to partially purify the SETD3-dependent activity for mass spectrometry analysis (Extended Data Fig. 1d-g). The ten most abundant hits in the proteomic dataset with molecular weights close to the candidate substrate (Extended Data Fig. 1h; Supplementary Table 1) were expressed as recombinant proteins and directly tested as SETD3 substrates *in vitro* (Fig. 1c). Of these proteins and other potential substrates, only beta-actin was methylated by SETD3 (Fig. 1c, Extended Data Fig. 1i). SETD6 and 10 additional active PKMTs do not methylate actin (Fig. 1d-e; Extended Data Fig. 1j). Also, SETD3 does not methylate the SETD6 substrate RelA (Fig. 1d)[6]. These data identify SETD3 as the first example of an enzyme to methylate actin *in vitro*.

To identify the specific actin residue/s modified by SETD3, *in vitro* methylated actin was analyzed by tandem mass spectrometry (MS/MS); deuterated SAM was used as the methyl

donor to distinguish SETD3-catalyzed methylation from all other sources. Unexpectedly, no lysine methylation events on actin were observed (Extended Data Fig. 2). We therefore extended the analysis to search for methylation events at other residues (arginine, glutamine, cysteine and histidine) and unambiguously identified incorporation of a single deuterated methyl moiety at histidine 73 of actin (Extended Data Fig. 3a-c). Histidine methylation is known to exist on a limited number of proteins. The only known histidine methyltransferase is the yeast enzyme Hpm1p, which methylates Rpl3 (not actin) and bears no structural resemblance to SETD3[7,8]. However, methylation of actin at histidine 73 (actin-H73me) is a canonical modification present in mammals but not in yeast[1,7,9]. We identified H73me (or equivalent) on actin purified from ten different model organisms ranging from worms to plants to humans, which all have a SETD3 homologue, but not in *S. cerevisiae*, which lacks SETD3 (Extended Data Fig. 4). Thus, actin-H73me is an evolutionarily conserved modification present in a broad range of multicellular eukaryotic organisms.

Mutation of actin H73 to alanine (H73A) prevents methylation by SETD3 (Fig. 2a). Histidine can potentially be methylated on the nitrogen in position 1 (π, *N1*) or 3 (τ, *N3*) of the imidazole ring (Fig. 2b), with His(3-me) the physiologic modification found on endogenous actin. Methylation assays performed on actin peptides spanning H73 (residues 66-80 of beta-actin) and in which H73 was either unmethylated or methylated at the *N1* or *N3* position (Extended Data Fig. 3d) showed that SETD3 methylated the unmodified peptide (k_{cat} 0.4 min^{-1}) and the peptide harboring H73(1-me) (with a much slower rate), but not H73(3-me), indicating that SETD3 catalyzes methylation of H73 at the physiologically relevant *N3* position (Fig. 2c; Extended Data Fig. 3e-g).

To gain insight into the molecular basis of how SETD3 methylates a histidine substrate, we co-crystallized SETD3 with an actin peptide (residues 66-80) containing H73 in the presence of *S*-adenosyl-L-homocysteine (SAH). We obtained three highly similar crystal forms, focusing on the highest resolution structure of 1.69 Å (Extended Data Table 1). SETD3 contains two lobes (SET and LSMT-like) forming a V-shaped cleft (Extended Data Fig. 5a). The 15-residue actin-peptide occupies an extended surface groove of the SET-domain (Fig. 2d), with H73 inserted into the active-site channel positioned to meet SAH from the other end (Fig. 2e). From the viewpoint of the cofactor-binding pocket, the methyl-accepting H73 *N3* atom is seen at the bottom of the channel (Extended Data Fig. 5b). Structural superimposition comparing SETD3 and SETD6[5] reveals that for SETD3, the methyl donor group of SAM points toward and is within the distance of 1.8 Å of the target *N3* atom of the imidazole ring (Fig. 2f). An intra-molecular hydrogen bond between the main-chain carbonyl oxygen of E72 and the main-chain amide nitrogen of I75 bends the peptide substrate in a sharp turn at H73. This configuration allows H73 and G74 (the smallest residue) to enter deep into the channel and positions the target *N3* atom in line with the methyl group and sulfur atom of SAM (Fig. 2f; Extended Data Fig. 5c-d); a linear arrangement comprising the nucleophile, the methyl group and the leaving thioester group in the transition state is required for the S_N2 reaction mechanism used by SAM-dependent methyltransferases[10].

All 15 residues of the actin peptide are bound in the structure (Fig. 2d; Extended Data Fig. 5d), with the SETD3-actin peptide interface consisting of an extensive network of charged/

polar and hydrophobic interactions involving both inter- and intra-molecular contacts (Extended Data Fig. 5d-n). For example, W79 and I71 of actin each fit into hydrophobic pockets on the SETD3 surface (Fig. 2g). This long and ordered peptide-substrate recognition groove for SETD3 is unique compared to other SET domains[11], suggesting that SETD3 would inefficiently accommodate substrates diverging from actin. Structure-guided point mutations in actin that disrupt the hydrophobic interaction (I71A) or are predicted to interfere with proper positioning of H73 in the catalytic pocket (G74I) impair the ability of SETD3 to methylate actin-H73, and the double mutant (I71A/G74I) abolishes activity (Fig. 3a). Further, while a W79E substitution is tolerated (Extended Data Fig. 5e), SETD3 has no activity on actin I71A/W79E double mutations (Fig. 3a). These data highlight the sensitivity of SETD3 activity on actin to changes in the sequence spanning H73. Indeed, the fifteen-residue sequence spanning H73 is highly conserved amongst the six human actin isoforms[9,12] with the only difference being an I/V variation at position 76 that does not impact SETD3 recognition (Extended Data Fig. 5g,o). Accordingly, all actin isoforms are methylated by SETD3 *in vitro* (Fig. 3b). Finally, the putative SETD3 catalytic mutant is a conserved tyrosine (Y312) that participates in forming the active-site pocket (Extended Data Fig. 5d,i,p). This mutant has residual activity; however, mutation of additional conserved residues important for SAM binding abolished SETD3 activity (Fig. 3c; Extended Data Fig. 5p).

We next raised a state-specific actin-H73me antibody that selectively recognized H73(3-me) peptides (Extended Data Fig. 6a). The majority of endogenous actin is marked by H73 methylation in HT1080 cancer cells and the depletion of endogenous SETD3 by two independent single guide RNAs (sgRNAs) results in almost complete loss of this modification as determined by Western blotting and mass spectrometry (Fig. 3d; Extended Data Fig. 6b). We also observed complete loss of actin-H73me in a clonal HeLa cell line in which the SETD3 alleles were disrupted (Fig. 3e; Extended Data Fig. 6c). Further, complementation of SETD3-depleted HT1080 cells with CRISPR-resistant wild-type, but not catalytically-dead SETD3$_{NHY}$, reconstituted actin methylation at H73 (Fig. 3f; Extended Data Fig. 6d). To assess the physiologic role of SETD3 in regulating actin H73 methylation, we obtained *Setd3*$^{+/-}$ mice from the Canadian Mouse Mutant Repository[13] and generated *Setd3* null homozygotes (*Setd3*$^{-/-}$), which are viable. Analysis of actin purified from nine different tissue types isolated from *Setd3*$^{+/+}$ and *Setd3*$^{-/-}$ mice showed that in tissues expressing SETD3, the majority of actin is methylated, however, this modification is not detected in any tissue from SETD3 deficient mice (Fig. 3g; Extended Data Fig. 7a-d). Finally, quantitative profiling of serum amino acids identified depletion of 3-methyl histidine as the lone abnormality in *Setd3*$^{-/-}$ mice (Extended Data Fig. 7e). Collectively, these results identify SETD3 as the physiologic actin-H73 methyltransferase.

Actin is one of the more abundant proteins in the human proteome and H73me is a high stoichiometry event. Our data argue that SETD3 is the principal enzyme tasked with generating actin-H73me, however is actin-H73 the only SETD3 substrate or one of many substrates? There are few known histidine methylated proteins besides actin – one is myosin, which SETD3 does not methylate (Fig. 3h). In addition, SETD3 has no activity on histones and several other proteins (see Fig. 1c-d and Extended Data Fig. 1i). To investigate SETD3 catalytic specificity in a physiologic and unbiased setting, we used quantitative

proteomics to compare the methylome of HeLa cells ±SETD3 (see Fig. 3e). Of the >900 methylation events detected in the analysis, including ~180 histidine methylated peptides (Supplementary Table 2), actin-H73me was the only modification quantitatively altered upon SETD3 depletion (Fig. 3i). Together, these results argue that the principal physiologic enzymatic function of SETD3 is actin-H73 methylation.

Based on elegant studies leveraging actin mutants, H73 and its methylation are suggested to influence actin polymerization dynamics, in part due to its proximity to the ATP binding site[9,12,14]. However, a direct side-by-side comparison of the properties of actin ±methylation has not previously been possible. We purified actin ±H73me (Extended Data Fig 8a-b) from HeLa cells (see Fig. 3e) and found that methylation promoted actin polymerization kinetics *in vitro* but did not affect depolymerization (Fig. 4 a; Extended Data Fig. 8c). Moreover, the rate of ATP nucleotide exchange was faster with the unmethylated species (Fig. 4b). We note that actin-H73me exhibited a subtle increase in polymerization when extending off of phalloidin-actin seeds, and made little difference on polymerization rates in response to Arp2/3 stimulation (Extended Data Fig. 8d-e). To explore the role of H73 methylation during actin polymerization in cells, mouse embryonic fibroblasts (MEFs) were isolated from *Setd3*^{+/−} mice positive for actin-H73me and *Setd3*^{−/−} mice lacking methylation (Fig. 4c). Cells containing actin-H73me were modestly more efficient at migration than cells deficient for methylated actin (Fig. 4d; Extended Data Fig. 8f). Together, these data are consistent with a model where SETD3 methylation of actin positively regulates actin polymerization in cells.

While *Setd3*^{−/−} MEFs show a defect in cell migration, *Setd3*^{−/−} mice are viable. Thus, actin-H73me must play a specialized physiologic role *in vivo* that is not essential for basal actin functions. The characterization of SETD3 knockouts by the International Mouse Phenotypic Consortium scored several phenotypes, including moderate skeletal muscle myopathy, abnormal cardiac EKG, and mild decreased lean mass[13]. We did not observe gross histopathologic changes in muscle tissue from young adult *Setd3*^{−/−} mice (Extended Data Fig. 9a-b). While we have not performed a comprehensive phenotypic analysis, we have observed that the litter size of female *Setd3*^{−/−} mice, regardless of the genotype of the sire, are significantly smaller than litters from *Setd3*^{+/+} and *Setd3*^{+/−} females (Extended Data Fig. 9c). To explore this observation further, we analyzed parturition in *Setd3*^{−/−} or littermate control females all sired by wild-type males. Normal parturition was defined as birth at 19 days post-coitum (dpc) and dystocia (delayed parturition) was defined as either no births (20 dpc) or incomplete delivery with fetuses remaining *in utero* (20 dpc). Dystocia, a rare phenotype, was observed in 8/9 *Setd3*^{−/−} mice, whereas normal parturition was observed in all of the control mice (Fig. 5a). As expected, in control mice, no fetuses were detected *in utero* at 20 dpc (Fig. 5b). In contrast, *Setd3*^{−/−} females typically had many fetuses remaining *in utero* at 20 dpc (Fig. 5b-c).

The dystocia observed in the *Setd3*^{−/−} females is independent of the genotype of the fetus as (1) wild-type males were used as sires, (2) pups successfully born to *Setd3*^{−/−} mice were viable, and (3) *Setd3*^{+/−} females had normal parturition. Thus, the cause of dystocia is of maternal origin. Secondary maternal dystocia is unlikely as there were no obvious and consistent anatomical pelvic abnormalities present in *Setd3*^{−/−} females, and

an anatomic defect would not explain the presence of intact fetuses *in utero*. Thus, the dystocia is primary, either due to abnormal myometrium contraction or a defect in hormone signaling. To distinguish between these possibilities, early labor was induced in wild-type and *Setd3*^{−/−} females with oxytocin administration at 18 dpc (see schematic Fig. 5d). Wild-type mice went into early labor and all pups were born within 24 hours of treatment, whereas the dystocia of *Setd3*^{−/−} mice was refractory to oxytocin (Fig. 5e-f). Similar results were observed with prostaglandin treatment as an independent ecbolic agent[15] (Extended Data Fig. 9d-e). These data identify a specific requirement for SETD3 in the contraction mechanism of the laboring uterus, a mechanism that fundamentally relies on proper actin behavior[16].

As multiple, unique point mutations in actin are implicated in the etiology of several human smooth muscle myopathies[17,18], we postulated a link between actin-H73me and uterine cell contraction in the primary dystocia of *Setd3*^{−/−} females. To test this idea, we depleted SETD3 and actin-H73me from primary human myometrial cells (Fig. 5g) and measured cellular contraction under normal conditions and in response to two uterine smooth muscle contraction stimulants. While depletion of SETD3 had only a marginal impact on intrinsic contraction, the absence of SETD3 significantly impeded signal-induced contraction by oxytocin and Endothelin-1 (Fig. 5h-i). Finally, the loss of Endothelin-1-induced cellular contraction upon SETD3 knockdown was rescued in the primary human myometrial cells by complementation with CRISPR-resistant wild-type SETD3, but not by catalytically inactive SETD3$_{NHY}$ (Fig. 5j-k; Extended Data Fig. 9f). These data suggest a specific role for actin-H73me in signal-induced contraction of smooth muscle.

Here, we have identified SETD3 as the first known metazoan protein histidine methyltransferase and the enzyme responsible for generating the abundant and enigmatic actin-H73me. SETD3 represents the first SET domain family member to methylate a residue besides lysine, broadening the current framework of possible chemistries catalyzed by SET domains. Our analysis revealed histidine methylation – previously detected on only a handful of proteins – to be surprisingly common, observed with a frequency similar to that of protein lysine di- and tri-methylation[19]. Actin mutations are implicated in smooth muscle myopathies (e.g. [17,18]) including a case of a pregnant patient suffering from uterine muscle atony[20]. We postulate that SETD3 deficiency and loss of H73me presents like intrinsic actin mutations by altering actin responsiveness to polymerization cues, which leads to defects in smooth muscle contraction. H73me impact on actin-myosin interactions is marginal (Extended Data Fig. 9g-h), suggesting smooth muscle contraction regulation is mediated by a different mechanism. Specifically, besides the canonical actin-myosin pathway, there is a distinct role for dynamic actin polymerization in mediating mechanical force generation of smooth muscle[21]. In summary, our work identifies a functional role for mammalian histidine methylation in regulating actin and smooth muscle contraction and suggests a broad role for this modification in the regulation of mammalian proteomes.

Methods

Reagents.

Biotinylated peptides were synthesized at the UNC High-Throughput Peptide Synthesis and Array Facility (Chapel Hill, NC)[22]. Fmoc-L-histidine amino acids with either (1-me) or (3-me) modifications (Sigma-Aldrich) were used in the synthesis of these peptides and synthesized peptides were purified by HPLC (>92% purity). Antibodies used in this study: SETD3 (Abcam), pan-actin (Cytoskeleton), beta-tubulin (Millipore), H3K4me2 (Cell Signaling), H3K36me2 (Cell Signaling), H73(3-me) see below, GFP (Invitrogen), Alexa488 anti-rabbit antibody (Life Technologies), anti-rabbit and anti-mouse peroxidase conjugated antibodies (Jackson Immunoresearch). Western blots were visualized by chemiluminescence (GE Healthcare).

Anti-H73(3-me) specific antibody generation.

Peptide corresponding to beta-actin amino acids 68-78 (KYPIEHGIVTN) with H(3-me) installed at position 73 was synthesized and HPLC purified (99% purity). This peptide was conjugated to KLH and used as antigen to immunize rabbits. Rabbit protocols, peptide conjugation, immunization, and antiserum production were performed by Pocono Rabbit Farm & Laboratory (Canadensis, PA). Antiserum was negatively selected against unmodified actin peptide (amino acids 66-80). Final purification with was performed with immobilized antigenic peptide to select for H73(3-me) specific antibodies.

Recombinant protein expression for *in vitro* reactions.

SETD3 (Q86TU7) and actin were cloned into pGEX-6P-1. MLL2 catalytic complex contained GST-tagged catalytic SET domain of MLL2, and full-length, 6xHis-tagged ASH2L, WDR5, DPY30, and RBBP5 that were all individually expressed in bacteria and assembled in stoichiometric proportions to result in a catalytic complex[23]. Lysine methyltransferases used as controls were reacted with previously reported substrates[24-35]. Candidate substrate cDNAs were subcloned from the human ORFeome (Open Biosystems) using an LR recombination reaction (Life Technologies) into pDEST15. Mutations of all proteins were generated using Phusion site-directed mutagenesis (Thermo Scientific) according to manufacturer's recommendations. All proteins were expressed as N-terminal GST fusions (except for non-catalytic MLL complex components) in BL21 or BL21(DE3) codon plus bacteria. Expression was performed at 16°C overnight in the presence of 0.1 mM IPTG. Recombinant GST fusions were purified with Glutathione Sepharose 4B (GE Healthcare) and eluted in 100 mM Tris pH 8.0, 10 mg/ml reduced glutathione (Sigma-Aldrich). Any cleavage of GST tags was performed with Prescission protease (GE Healthcare) overnight at 4°C. Recombinant 6xHis-tagged proteins were purified with Ni-NTA agarose (Life technologies) and eluted in 100 mM Tris pH 8.0, 250 mM imidazole. Kinetics experiments and crystallography utilized additional purification described below.

Purification of SETD3 for crystallography.

SETD3 was expressed as a GST-fusion as described above. Cleared bacterial lysate containing soluble glutathione S-transferase (GST) fusion SETD3 was first loaded on a

self-packed glutathione-sepharose column and eluted with buffer containing 100 mM Tris (pH 8.0), 150 mM NaCl, 5% glycerol, 0.5 mM TCEP and 20 mM reduced glutathione. The GST tag was removed by ~100 μg prescission protease (purified in-house) at 4°C overnight. The cleaved protein solution was diluted to ~50 mM NaCl and further purified by HiTrap Q-HP, GE Healthcare) with a linear gradient of 50 mM to 500 mM NaCl; SETD3 eluted together with the cleaved GST around 200-300 mM NaCl. To remove GST, fractions were loaded onto a fresh glutathione-sepharose column and the flow-through was collected and concentrated to ~2 ml. SETD3 was then further purified by size exclusion chromatography (Superdex 200, GE Healthcare) in 20 mM Tris (pH 8.0), 200 mM NaCl, 5% glycerol, 0.5 mM TCEP. All purification steps were performed at 4°C. The chromatography was conducted in a BIO-RAD NGC™ system.

Cellular fractionation.

Cytoplasmic cellular extracts were prepared by established protocols[36]. Briefly, cells were disrupted by hypotonic lysis (25 mM KCl, 1.5 mM $MgCl_2$, 10 mM HEPES–KOH pH 7.9, protease inhibitors) and dounce homogenization. Size exclusion chromatography (Superose 6) was performed in hypotonic lysis buffer. Ion-exchange chromatography (Sepharose Q HP) columns were equilibrated in hypotonic lysis buffer and proteins were eluted on a linear gradient from 25-600 mM KCl. Fractions were concentrated with centrifugal filter units (Amicon, 3000 Da MWCO) before being used as substrate in *in vitro* reactions with radiolabeled SAM. Chromatography for substrate enrichment was performed with an AKTA FPLC (GE Healthcare)

In vitro methylation reactions.

In vitro methyltransferase reactions were performed with 5 μg methyltransferase, 1 μg substrate, and 2 μCi ^{3}H-*S*-adenosylmethionine (American Radiolabeled Chemicals) in a buffer containing 50 mM Tris pH 8.0, 20 mM KCl, 5 mM $MgCl_2$ at 30°C overnight. Reactions were resolved by SDS-PAGE, and ^{3}H-methylation was visualized by autoradiography and gels were stained with Coomassie as a loading control. Reactions with deuterated SAM (CDN Isotopes) or normal SAM (Sigma-Aldrich) were performed with SAM at a final concentration of 80 μM.

Steady-state kinetic measurement.

Human beta-actin peptide (residues 66-80; TLKYPIEHGIVTNWD) was used as a substrate for SETD3. The reaction mixture containing 20 mM Tris (pH 8.0), 50 mM NaCl, 0.1 mg/ml BSA, 1 mM DTT, and 0.18 μM SETD3. To determine the Km value for peptide, the concentration of S-adenosyl-L-methionine (SAM) was kept constant at 40 μM, while for determination of the Km for SAM, peptide concentration was kept constant at 50 μM. Reactions were carried out at room temperature for 20 min with a total volume of 20 μl, and terminated by the addition of trifluoroacetic acid (TFA) to 0.1% (v/v). The activity of SETD3 was measured using a bioluminescence assay (MTase-Glo™, Promega) in which the reaction by-product S-adenosyl-homocysteine (SAH) is converted into ATP in a two-step reaction and can be detected via a luciferase reaction[37]. In general, 5 μl of reaction mixture was transferred to a low-volume 384-well plate and the luminescence assay was

performed according to the manufacture's protocol. A Synergy 4 Multi-Mode Microplate Reader (BioTek) was used to measure luminescent signal.

Time-course of methylation for three β-actin peptides.

Typically, a reaction mixture contained 20 mM Tris (pH 8.0), 50 mM NaCl, 0.1 mg/ml BSA, 1 mM DTT, 40 μM SAM and 50 μM peptide. In addition to the unmodified peptide, 1-methyl-His and 3-methyl-His peptides were used in the activity assay. For unmodified peptide, 0.18 μM SETD3 was used, while for modified ones, 80-fold higher amounts of SETD3 (14.4 μM) were used due to very low activity on these peptides. For each time point, 10 μl of reaction mixture was taken and adding TFA to 0.1% stopped the reaction. The luminescence assay was performed as described above.

Mass spectrometry.

LC-MS/MS was performed using an Orbitrap Elite or Fusion (Thermo Scientific) and data was analyzed manually or using MaxQuant software[38]. Peptide identification searches with MaxQuant were performed with parameters to identify methionine oxidation, N-acetylation, monomethyl lysine, dimethyl lysine, trimethyl lysine, methyl histidine, monomethyl arginine, dimethyl arginine, methyl glutamine, and methyl cysteine. *in vitro* reactions were directly resolved by SDS-PAGE before mass spectrometry analysis was performed as above and digested with trypsin, chymotrypsin or Glu-C (Promega). Quantitative proteomic analysis was performed with SILAC, light isotopic labels (K0R0) and heavy isotopic labels (K8R10). In the SETD3-dependent methylomics, no peptides with a SILAC ratio greater than 1.5 were deemed to be SETD3-dependent methyl events. No peptides (other than actin) with at least a 1.5-fold ratio in the reverse direction and NaN ratio in the forward direction were identified at all in the forward direction. Actin H73 methylation was detected with light (WT cells, K0R0) labeling in the forward direction and not with heavy labeling (SETD3 knockout cells, K8R10). We thus concluded that the lack of a calculable ratio (light/heavy) in the forward direction is due to the clonal nature of the cell lines being used. We therefore plotted the forward ratio as infinite (Fig. 3i).

Targeted quantification of actin methylation was performed by manual identification of methylated and unmethylated peptides followed by integration of area under the curve for chromatographic peaks associated with the corresponding *m/z*. Percentage of methylated peptides was determined as a fraction of the sum total area for methylated and unmethylated species. Actin was isolated from cellular or tissue sources using DNAse I affinity chromatography[39]. DNAse I was immobilized to NHS-activated Sepharose FF (GE Healthcare) overnight in 100 mM Hepes pH 7.5, 150 mM NaCl, 80 mM $CaCl_2$. Cells/tissues were homogenized with buffer containing 1M Tris pH 8.0, 600 mM KCl, 0.5 mM $MgCl_2$, 4% NP-40, 1% Tween-20, 1 mM DTT, 1 mM ATP, and protease inhibitors[40] (Roche). Cleared lysates were incubated with immobilized DNase I resin overnight, washed, boiled in SDS sample buffer, and purified actin was resolved by SDS-PAGE. Gels were silver-stained (Thermo Scientific) then actin bands were excised and processed for mass spectrometry by in-gel digest with sequencing grade trypsin. The following sources were used in the analysis of actin methylation across evolution: *S. cerevisiae*, mid-log BY4741; *A. thaliana*, leaf tissue; *N. benthamiana*, leaf tissue; *C. elegans*, mixed population; *D. melanogaster*, larvae;

S. frugiperda, Sf9 cells; *D. rerio*, 5 days post fertilization embryos; *X. laevis*, egg extract; *G. gallus*, skeletal muscle; *M. musculus*, brain/uterine/skeletal muscle tissue; *H. sapiens*, cell lines.

Crystallography.

Crystallization of the SETD3-SAH-actin peptide (residues 66-80; Genscript) complex was carried out by the hanging-drop vapor-diffusion method at 20°C after mixing SETD3 (~15 mg/ml) with SAH and peptide at a molar ratio of 1:4:5, and then mixed with an equal amount of well-solution. Three different crystal forms were obtained. Crystals with space group $P2_1$ were obtained with 0.2 M ammonium acetate, 0.1 M sodium citrate tribasic dihydrate pH 5.6, and 30% (w/v) polyethylene glycol 4000. Crystals with space group $P2_12_12_1$ were obtained with two similar conditions, either 0.2 M ammonium sulfate or 0.2 M sodium chloride, 0.1 M BIS-TRIS pH 5.5, 25% (w/v) polyethylene glycol 3350, and 0.1 M BIS-TRIS pH 5.5, 25% (w/v) polyethylene glycol 3350. The first form, like the $P2_1$ crystal, contained two SETD3-SAH-peptide complexes per asymmetric unit, while the second contained only one complex.

For X-ray diffraction data collection, single crystals were flash frozen in liquid nitrogen by equilibrating in a cryoprotectant buffer containing well solution with 25% (v/v) ethylene glycol. All datasets were collected at the SER-CAT beamline 22ID of Advanced Photon Source at Argonne National Laboratory. Crystallographic datasets were processed with HKL2000[41]. Molecular replacement was performed with PHENIX PHASER module[42] by using the structure of human SETD3 in complex with SAM (PDB ID 3SMT) as a search model. PHENIX REFINE[43] was used for refinement with 5% randomly chosen reflections for validation by the Rfree value. COOT[44] was used for peptide building and model corrections between refinement rounds. Structure quality was analyzed during PHENIX refinements and later validated by the PDB validation server. Molecular graphics were generated using PyMol (Schrödinger, LLC).

We note that the high-resolution data at 1.69 Å (PDB 6MBK) were the result of merging two datasets collected from two different parts of the same crystal. This crystal did diffract X-rays to higher resolution but was susceptible to radiation damage, especially in the higher resolution range. The merge resulted in 98.4% completeness in the highest resolution shell of 1.75-1.69 Å. The somewhat higher R-work and R-free values of the structure (PDB 6MBK) might be an indication of radiation damage that could not be modeled and further refinement would not lower these R values substantially and the structure and map compared well with the quality of the other two crystal forms.

Actin purification for biochemical assays.

Actin was purified from wild-type HeLa cells or a clonally-derived HeLa cell line in which SETD3 was knocked out. Purification was adapted from established protocols[45]. Briefly, HeLa cells were resuspended in lysis buffer (10 mM Tris–HCl, pH 8.0, 11.6 % (w/v) sucrose, 1 mM EGTA, 1 mM ATP, 5 mM (DTT), and protease inhibitor cocktail) and lysed by sonication. Lysates were cleared by ultracentrifugation (100,000 × g, 2 hours). Cleared cellular extract was loaded onto an anion-exchange column (Sepharose Q HP, GE

Healthcare) equilibrated with column buffer (10 mM Tris–HCl, pH 8.0, 0.2 mM $CaCl_2$, 0.5 mM ATP, 0.5 mM DTT). Actin protein was eluted on a linear gradient of column buffer containing 0 mM KCl to column buffer containing 600 mM KCl. Actin-positive fractions were polymerized with 2 mM $MgCl_2$ and 1 mM ATP at room temperature, and polymerized actin was pelleted at $100,000 \times g$ for 2 hours. F-actin was resuspended and depolymerized in 2 mM Tris pH 8.0, 0.2 mM $CaCl_2$, 0.5 mM DTT, and 0.2 mM ATP for 2 days. Residual F-actin was cleared by ultracentrifugation as before and the protein in the supernatant was used in biochemical assays.

Pyrene-based polymerization assays were performed according to commercially available kit instructions (Cytoskeleton). Purified HeLa actin was combined in a 10:1 ratio with pyrene-labeled actin from rabbit skeletal muscle (Cytoskeleton). Polymerization was induced with 2 mM $MgCl_2$, 50 mM KCl, and 1 mM ATP and monitored by fluorescence in a plate reader (excitation: 355 nm/emission: 410 nm, Biotek Cytation 3, Gen5 v3.04.17 software). Readings were taken every 60 seconds with orbital shaking. Depolymerization assays were performed by diluting actin polymerized as above 250-fold in 10 mM Tris pH 8.0, 0.2 mM $CaCl_2$, 1 mM ATP. Depolymerization was monitored by fluorescence similar to polymerization. Phalloidin-actin seeds were made by polymerizing monomeric actin into filaments followed by incubation of the resulting F-actin with a stoichiometric excess of phalloidin (Millipore-Sigma). F-actin was pelleted for 1h at $100,000 \times g$. The F-actin was washed and resuspended in F-buffer (10 mM Tris pH 7.5, 2 mM $MgCl_2$, 50 mM KCl, 1 mM ATP, 1 mM DTT) and then sheared through a 27G needle. Seeds were allowed to recover overnight at room temperature. Polymerization with seeds was performed with 2 μM seed, 1 μM monomeric actin, and 0.1 μM pyrene-actin. Polymerization with Arp2/3 complex (Cytoskeleton) and recombinant WASP VCA (Cytoskeleton) were used at concentrations of 5 nM and 100 nM respectively with 1 μM actin and 0.1 μM pyrene-actin.

Nucleotide Exchange.

Nucleotide exchange assays were performed as previously reported[46]. G-actin monomers were transferred into a buffer without ATP (2 mM Tris pH 7.5, 0.2 mM $CaCl_2$, 1 mM DTT) by desalting column (GE Healthcare, PD spin column with G-25). 1,N^6-ethenoadenosine-5'-O-triphosphate (ε-ATP, Axxora) was added to G-actin at a final concentration of 0.3 mM and incubated on ice for at least 2h. Unbound ε-ATP was removed by desalting as before. ATP exchange of ε-ATP with normal ATP (100 μM) was performed with 2 μM G-actin and monitored by fluorescence (excitation, 340 nm; emission, 410 nm) in triplicate.

Cell culture.

293T (ATCC), HT1080 (ATCC) and H1-HeLa (ATCC) cells were cultured in Dulbecco's Modified Eagle's Medium (DMEM, Life Technologies) supplemented with 10% Fetal bovine serum, 2 mM L-glutamine, and penicillin/streptomycin (Life Technologies). Primary uterine smooth muscle cells (ATCC) were cultured in vascular cell basal media (ATCC) supplemented with the vascular smooth muscle growth kit (ATCC). All above cell lines were authenticated and declared mycoplasma free by ATCC. Transfections were performed with either TransIT-293 or TransIT-LT1 (Mirus) in 293T cells or HT1080 cells, respectively. Stable cell lines were generated using lentiviral transductions. 293T cells

were co-transfected with lentiviral plasmid, pCMV- 8.2 and pCMV-VSVg in a ratio of 9:8:1 by mass. 48 hours after transfection, target cells were transduced with 0.45 μm filtered viral supernatant supplemented with 8 μg/ml polybrene. Viral concentration was performed as necessary with Lenti-X lentiviral concentration solution per manufacturer's recommendations (Takara). Cells were selected 24 hours after media replacement. To deplete cells of SETD3, CRISPR/Cas9 components were stably expressed in HT1080 cells using lentiCRISPRv2 (Addgene) with the following single guide RNAs: sgControl, 5'-CTTCGAAATGTCCGTTCGGT-3'; sgSETD3-1, 5'-TGTTACAGAATGCAGCAGTC-3'; sgSETD3-2, 5'-GTATGTGCAGATCCGGACTC-3'. sgSETD3-1 was used for reconstitution experiments and generation of the clonal H1-HeLa cell line. Cell selection was performed with 2 μg/ml puromycin or 100 μg/ml hygromycin. SETD3 cDNA cloned into pLenti CMV Hygro DEST (W117-1) (Addgene) was made CRISPR/Cas9-resistant by incorporating a synonymous mutation into the PAM sequence associated with sgSETD3-1 from CGG to CTG. Reconstitution experiments were performed by transient transfection in HT1080 cells or stable incorporation by lentivirus in primary uterine smooth muscle cells. SILAC cell culture was performed with DMEM for SILAC (Thermo Scientific), supplemented with 10% dialyzed fetal bovine serum, 115 mg proline (Applichem), 50 mg lysine (light, lysine HCl [Applichem]; heavy, $^{13}C_6$,$^{15}N_2$-L-Lysine HCl [Silantes]), and 50 mg arginine (light, arginine HCl [Applichem]; heavy, $^{13}C_6$,$^{15}N_4$-L-Arginine HCl [Silantes]). Cells used for SILAC-based proteomics were cultured in SILAC media for at least one week before analysis.

Immunofluorescence imaging

H1-HeLa cells were seeded overnight onto autoclaved 12mm circle micro cover glass (VWR) at 50,000 cells per well in 24-well plates (Greiner Bio-One). Samples were fixed with 4% paraformaldehyde (Sigma) for 30 minutes at room temperature. Each sample was incubated with Anti-GFP antibody (1:300) in immunofluorescence blocking buffer (1× phosphate buffered saline (PBS) with 3% BSA, 1% saponin and 1% Triton X-100) overnight at 4°C. Cells were washed thoroughly with 1xPBS and then incubated for 1 hour at room temperature with Alexa488 anti-rabbit antibody (1:500) and DAPI stain (Insitus Biotechnologies, 1:300 dilution) in immunofluorescence blocking buffer. Washed micro cover glasses were then mounted onto microscope slides (Fisher Scientific) using Vectashield with DAPI (Vector Laboratories Inc). Images were taken with Zeiss LSM 700 confocal microscope and processed with Volocity software.

MEF cell line generation.

Embryos were harvested 13.5 dpc and internal organs were removed. Remaining embryos were minced and treated with trypsin to dissociate cells for 30 minutes at 37°C. Trypsinization was quenched with growth media (DMEM+10% fetal bovine serum). Quenched cell suspension was plated and allowed to grow for 4 days. At this point, cells were frozen or used in experiments. Genotyping of new cell lines were performed with residual embryonic tissue and confirmed by western blot analysis.

Cell Migration assays.

Cell migration assays were performed with Radius cell migration kits (Cell Biolabs). MEFs (1×10^5 cells) were plated in 24-well migration plates and allowed to attach overnight. The Radius gel was removed according the manufacturer's protocol. After gel removal, imaging was performed over a 24h period with a Nikon Eclipse Ti inverted fluorescent microscope and NIS elements (version 4.60) software. During image acquisition, the environmental conditions were kept at 5% CO_2 and 37°C (Okolab). After the 24 hour period, cells were fixed and stained with DAPI according to kit instructions. Cell migration was quantified by re-imaging migration fields and counting DAPI-stained nuclei within the boundary of the circular void left by the gel at 0h. Migration assays were performed in triplicate.

Cell Contraction assays.

Cellular contraction assays were performed on a collagen substrate (Cell Biolabs). 450 μl collagen mixture made with the provided 5xPBS was added to a 24-well plate and allowed to polymerize according to the manufacturer's protocol. Primary uterine smooth muscle cells (5×10^4 cells) were layered on top of a collagen matrix in vascular basal medium without the growth kit. Cells were allowed to attach to the collagen overnight at 37°C. The next day, the collagen disks were released from the sides of each well. Induction of contraction was performed with 10 μM oxytocin (Tocris) or 1 μM Endothelin-1 (Tocris). Contraction was monitored by imaging after 24h of contraction. Quantification of collagen disk area was performed in ImageJ (NIH). Relative disk area was determined by normalizing to the area of disks lacking cells. All assays were performed in triplicate.

Ethics statement

Mice were housed in the Stanford mouse facility accredited by the Association for Assessment and Accreditation of Laboratory Animal Care. All experiments were approved by Stanford's Institutional Animal Care and Use Committee.

Maintenance of mouse colonies.

Husbandry is performed in accordance with the *Guide for the Care and Use of Laboratory Animals, 8th edition* (2010) and the *2015* revision of the *Public Health Service Policy on Humane Care and Use of Laboratory Animals*. Room conditions included a temperature of 23°C, relative humidity of 30% to 40%, and a 12:12-h light:dark cycle (lights on, 0700 h). All mouse colonies are maintained under SPF conditions in irradiated disposable individually ventilated cages (Innocage[R], Innovive, San Diego, CA) with irradiated, corncob bedding, irradiated food (Teklad 2918 Global 18% Protein Rodent Diet, Envigo) and UV-irradiated, acidified (pH, 2.5 to 3.0), reverse-osmosis–purified bottled water (Aquavive[R], Innovive). The mouse colonies are monitored for viral, bacterial, and parasitic pathogens using dirty-bedding sentinels that were tested quarterly and were found to be free of mouse parvovirus, minute virus of mice, mouse hepatitis virus, mouse rotavirus, Theiler's murine encephalomyelitis virus, murine norovirus, Sendai virus, mouse adenovirus 1 and 2, ectromelia virus, lymphocytic choriomeningitis virus, pneumonia virus of mice, respiratory enterovirus III, fur mites, lice, and pinworms. Sample size was maximized as much as possible to gain highest confidence in the results. No randomization was necessary as only

single variables changed per experiment. Blinding was not necessary as any phenotypic assessment or other measurements was performed using discrete, quantitative measurements

Mouse Strains.

C57BL/6N - $Setd3^{tm1.1(NCOM)Mfgc}$/Tcp heterozygous mice were obtained from the Canadian Mouse Mutant Repository (CMMR, Toronto, Canada). The strain was made at the Toronto Centre for Phenogenomics as part of the NorCOMM2 project using NorCOMM ES cells[47]. Progeny were genotyped using either the Setd3-McKerlie PCR assay to identify either the 212-bp wild-type band (primers: Setd3_wt_F1- AACCAGCAGTGCACAGAGACAAGCTG; Setd3_wt_R1 - AACCCAAACTCTGCCAGCCAAAGCAC) and/or a 566 bp tm1.1 band (primers: Setd3_tm1_F4- AAACTGGTGCTGCTGATAACCTGGGC; GH717 - CACCGACGCCAATCACAAACAC) following instructions provided by the CMMR or the use of a commercial genotyping service (Transnetyx, Memphis, TN). For timed pregnant matings, C57BL/6N male mice were purchased from Charles River Laboratories (Hollister, CA).

Quantification of litter size and length of gestation.

Quantification of pregnancies and litters for both trio or pair breeding females were tabulated for $Setd3^{-/-}$, $Setd3^{+/-}$, $Setd3^{+/+}$ females. All litters that were observed ("confirmed") were counted, even if pups subsequently died. To determine pups/litter, litters that were lost prior to when pups could be counted were listed as 0 pups for that litter. The length of gestation for $Setd3^{-/-}$, $Setd3^{+/-}$, $Setd3^{+/+}$ females was determined by timed pregnant matings. Females were mated to wild type C57BL/6N males (Charles River Laboratories, Hollister, CA). Whether the female was a virgin (primigravida) or had a previous pregnancy (multigravida) was recorded. Presence of a vaginal plug was denoted 0 day post coitum (dpc). Plugged females were moved to a separate cage and weights taken at intervals to confirm pregnancy. A few days prior to 19 dpc, the female was placed in a separate cage and provided with nesting material (Enviro-dri^R, Shepherd Specialty Papers) and a paper tube. Cages were checked for births twice daily (morning and afternoon) starting from 18 dpc.

Quantifying dystocia and fetuses *in utero*.

The day of parturition for $Setd3^{-/-}$ females varied from 19 dpc to 20 dpc. Normal parturition was defined as birth at 19 days post-coitum (dpc) and dystocia (delayed parturition) was defined as either no births (20 dpc) or incomplete delivery with fetuses remaining *in utero* (20 dpc). To determine whether $Setd3^{-/-}$ females that delivered on 19 dpc still exhibited a delayed in parturition, females were euthanized on late 20 dpc if they did not deliver on 19 dpc ($Setd3^{-/-}$) or 24h after giving birth if they delivered on 19 dpc ($Setd3^{-/-}$, $Setd3^{+/-}$, $Setd3^{+/+}$) and examined for the presence of fetuses *in utero*. We note that the dystocia occurred in both primigravida and multigravida $Setd3^{-/-}$ females and that actin-H73me is not detected in the uterus of late-stage pregnant $Setd3^{-/-}$ females (data not shown).

Induction of parturition.

Oxytocin (VetOne[R], MWI Veterinary Supply Co.) was given subcutaneously on 18 dpc to induce preterm labor (dose = 0.4 U in 0.9% saline supplemented with 0.1% calcium gluconate and 0.025% dextrose, given 3x, q30 min over a period of 1.5 h) to $Setd3^{-/-}$, and $Setd3^{+/+}$ timed-pregnant females. The normal day of birth for $Setd3^{+/+}$ mice of this strain is 19 dpc. All pups born on 18 dpc were removed and euthanized. All mice quantified for fetuses *in utero* were euthanized at 1700h on d19.

A PGF2α cocktail (1 ml Lutalyse[R] (5 mg PGF2α/ml), 1 ml 10% calcium gluconate, 0.05 ml of 50% isotonic dextrose, and 8.0 ml of 0.9% sterile saline) was used to induce parturition in two $Setd3^{-/-}$ females on 19 dpc. Females were injected subcutaneously with 1 ml of the cocktail at 3 time points on 19 dpc (~0900 h, ~1200 h, ~1700 h). The females were monitored for parturition and euthanized on late 20 dpc at 1700 h.

Metabolic analysis.

Amino acids were analyzed as underivatized compounds by liquid chromatography tandem mass spectrometry (LC-MS/MS). Samples (50μL) were deproteinized with 50μL of 6% sulfosalicylic acid, and centrifuged for 15 min at 17,000 RCF. Supernatants were diluted with an isotopic standard mixture (Cambridge Isotope Laboratories, Inc) in 2 μM tridecafluoroheptanoic acid (TDFHA), and then injected into the LC-MS/MS system. Samples were analyzed using a clinically validated amino acid analysis method[48]. An Agilent 1200 series liquid chromatography system equipped with a Thermo Hypercarb trap column (3 μm, 4.6 × 50 mm) and a Waters BEH C18 analytical column (2.5 μm, 2.1 × 100 mm) was used to separate compounds in a trap and reverse-elute configuration. An Agilent 6460 triple quadrupole mass spectrometer was used in positive polarity electrospray ionization for detection by dynamic multiple reaction monitoring (MRM). Mobile phase A was 0.02% perfluoroheptanoic acid and mobile phase B was acetonitrile. Standard curves were prepared by diluting amino acid standards (Wako Chemicals USA, Inc); for 1-methylhistidine, S-aminoethylcystine was used as the internal standard and for 3-methylhistidine, histidine-$^{13}C_6^{15}N_3$ was used as the internal standard. Agilent Masshunter B08 was used for data analysis.

Muscle Tissue Histology.

Tissues were fixed by immersion in 10% neutral buffered formalin, routinely processed for paraffin embedding, and 5μm thick sections were routinely stained with hematoxylin and eosin (H&E).

Myosin expression and purification

Construction, expression, and purification of the wild-type recombinant human beta-cardiac myosin sS1 and the hypertrophic cardiac myopathy H251N mutant[49] are described in detail elsewhere[49-51]. Briefly, a truncated version of MYH7 (residues 1–808), corresponding to sS1, with a C-terminal enhanced green fluorescent protein (eGFP), was co-expressed with myosin light chain 3 (MYL3), encoding human ventricular essential light chain (ELC), and containing an N-terminal FLAG tag (DYKDDDDK) and tobacco etch virus (TEV) protease site in mouse myoblast C2C12 cells using the AdEasy Vector System (Obiogene Inc.). The

myosin heavy chain with its associated FLAG-tagged ELC was first purified from clarified lysate with anti-FLAG resin (Sigma). After cleaving off the FLAG tag with TEV protease, the human beta-cardiac sS1 was further purified using anion exchange chromatography on a 1-mL HiTrap Q HP column (GE Healthcare). Peak fractions were eluted with column buffer (10 mM imidazole, pH 7.5, ~200 mM NaCl, 4 mM MgCl2, 1 mM DTT, 2 mM ATP, and 10% sucrose) and concentrated by centrifugation in Amicon Ultra-0.5 10-kDa cutoff spin filters (EMD Millipore) before being used in assays or stored at −80 °C.

in vitro motility.

Experiments were conducted following previously described methods[51-54]. Briefly, frozen myosin protein was first subjected to a "deadheading" procedure to remove inactive heads. Myosin was mixed with 5 – 10x molar excess of unlabeled F-actin on ice for 5 min, followed by addition of 2 mM ATP for 3 min, then centrifuged at 95k rpm in a TLA-100 rotor (Beckman Coulter) at 4°C for 20 min. The supernatant was collected for use in the motility. Flow chamber was built on a nitrocellulose-coated coverslip mounted on a glass slide. Deadheaded myosin was immobilized via specific binding to the GFP antibody that non-specifically binds to the coverslip surface, followed by blocking with assay buffer (25 mM imidazole pH 7.5, 25 mM KCl, 4 mM MgCl$_2$, 1 mM EGTA, 10 mM DTT, and 1 mg/ml BSA). A final solution containing fluorescently labeled bovine cardiac F-actin, 2 mM ATP, and an oxygen-scavenging system (0.4% glucose, 0.11 mg/ml glucose oxidase, and 0.018 mg/ml catalase) was subsequently flowed in before imaging on a total internal reflection fluorescence microscope (Nikon Eclipse Ti-E) equipped with a 561 nm laser (Cobolt) and a 100x oil-immersion objective (Nikon)[55]. Time-lapse movies were acquired at multiple fields of views for each experimental condition at 1 Hz sampling rate. Movies were analyzed using the FAST (Fast Automated Spud Trekker) software[56] to obtain the mean velocities with 20% tolerance. All experiments were conducted at 23°C.

Actin-activated Myosin ATPase activity.

Purified actin was freshly cycled to F-actin by extensive (four times over 4 d) dialysis in ATPase buffer (10 mM imidazole, pH 7.5, 5 mM KCl, 3 mM MgCl2, and 1 mM DTT) to remove any residual ATP. The monomeric concentration of F-actin was determined by measuring the absorbance of a serial dilution of the actin in 6 M guanidine hydrochloride both at 290 nm with an extinction coefficient of 26,600 $M^{-1}cm^{-1}$ and at 280 nm with an extinction coefficient of 45,840 $M^{-1}cm^{-1}$ in a spectrophotometer (NanoDrop). Full-length human gelsolin was added to actin at a ratio of 1:1,000 to reduce the viscosity of the actin and thereby decrease pipetting error at higher actin concentrations without affecting the ATPase activity. The steady-state actin-activated ATPase activities of freshly prepared human beta-cardiac sS1-eGFP myosin using WT and KO actin were determined using a colorimetric readout of phosphate production[57], as described in a previous work[51]. In this assay, reactions containing sS1 at a final concentration of 0.01 mg/ml, 2 mM ATP, and actin at concentrations ranging from 5 to 77 μM were performed at 23 °C with shaking using a microplate spectrophotometer (Thermo Scientific Multiskan GO). The rate of sS1 activity was obtained by linear fitting the phosphate signal as a function of time and converted to activity units using a phosphate standard. Each actin condition was performed in duplicate, The error on each data point represents the s.e.m. of the duplicates. The Michaelis–Menten

equation was fitted to determine the maximal activity (kcat) and the actin concentration at half-maximum (apparent Km for actin).

Statistics.

GraphPad Prism 7.0 or KaldeidaGraph 4.5 software were used for statistics.

Data availability.—The X-ray structures (coordinates and structure factor files) of SETD3 with bound actin peptide have been submitted to PDB under accession number 6MBJ (P21), 6MBK (Two complexes in P212121) and 6MBL (one complex in P212121). Source data for this study are provided as supplementary information (Fig. 4d, 5b, 5e, 5f, 5i, 5k; Extended Data Fig. 7e, 9c, 9h). Source gel data provided for cropped images (Fig. 1a, 1d, 1e, 2a, 2c, 3a-f,g, 4c, 5g, 5j; Extended Data Fig. 1b) is provided in Supplementary Figure 1. Mass spectrometry data associated with Fig. 1c/Extended Data Fig. 1h and Fig. 3i are provided as a Supplementary Tables. Additional requests can be made to the corresponding authors.
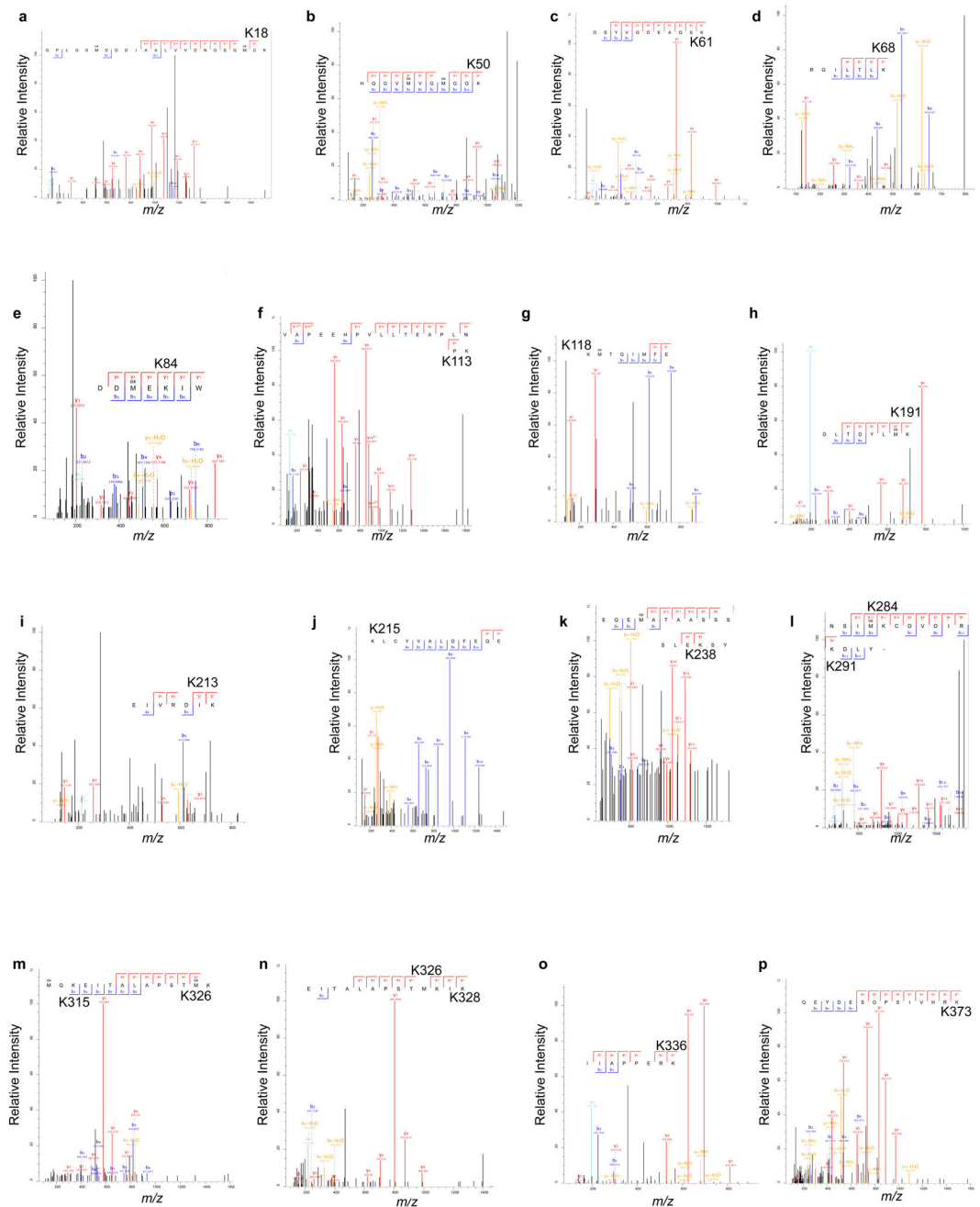
Extended Data
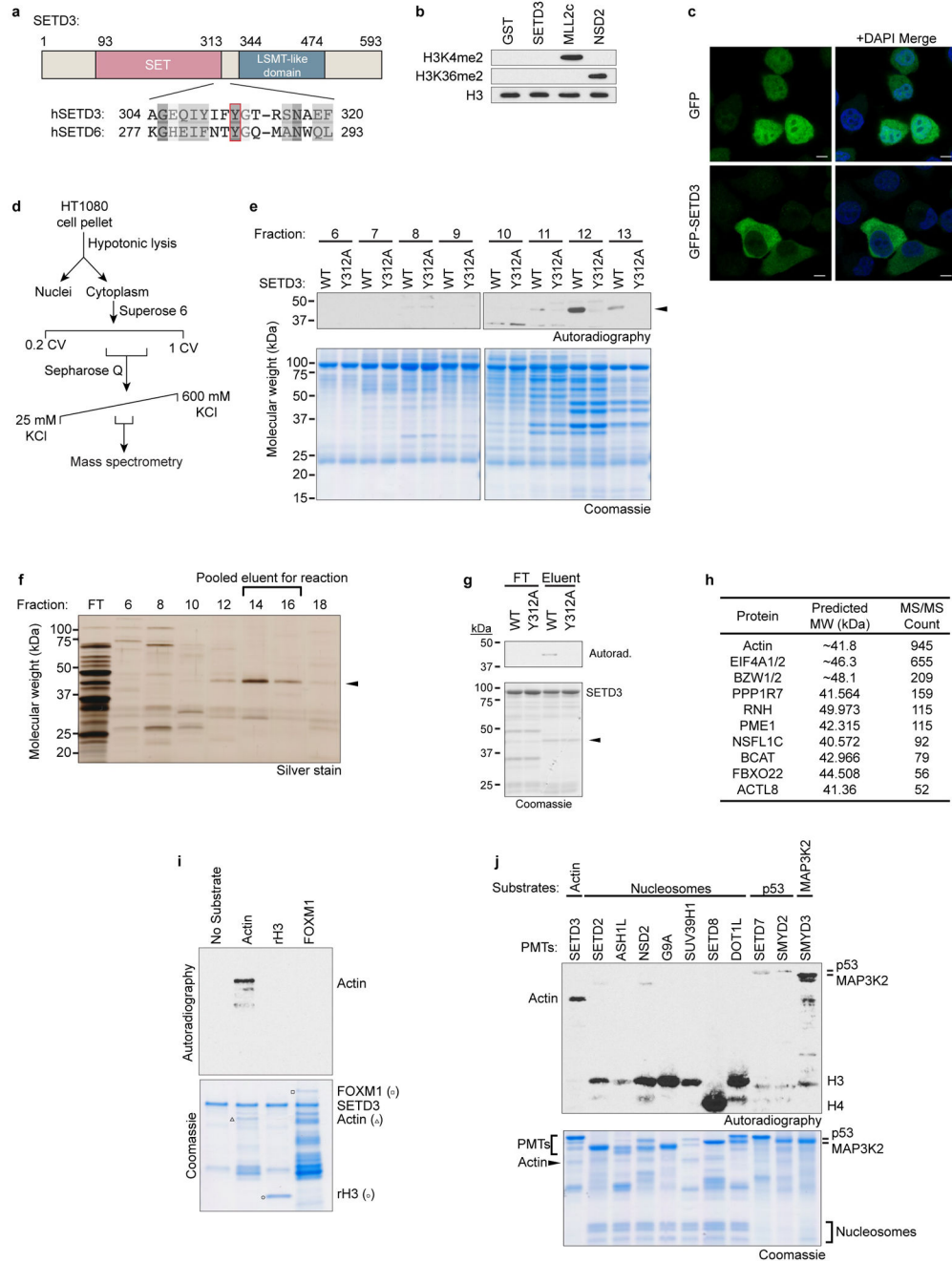
Extended Data Figure 1. Identification of actin as a SETD3 substrate.
a, *Top:* domain structure of SETD3 containing an N-terminal SET domain and a C-terminal domain homologous to plant Rubisco LSMT. *Bottom:* alignment of homologous methyltransferases human SETD3 and human SETD6. Red box, putative catalytic tyrosine.
b, Methylation reactions as in Fig. 1a with non-radiolabeled SAM and analyzed by Western blot with indicated antibodies. Total H3 shown as a loading control. **c,** SETD3 localizes to the cytoplasm. Representative immunofluorescence images of GFP or GFP-SETD3
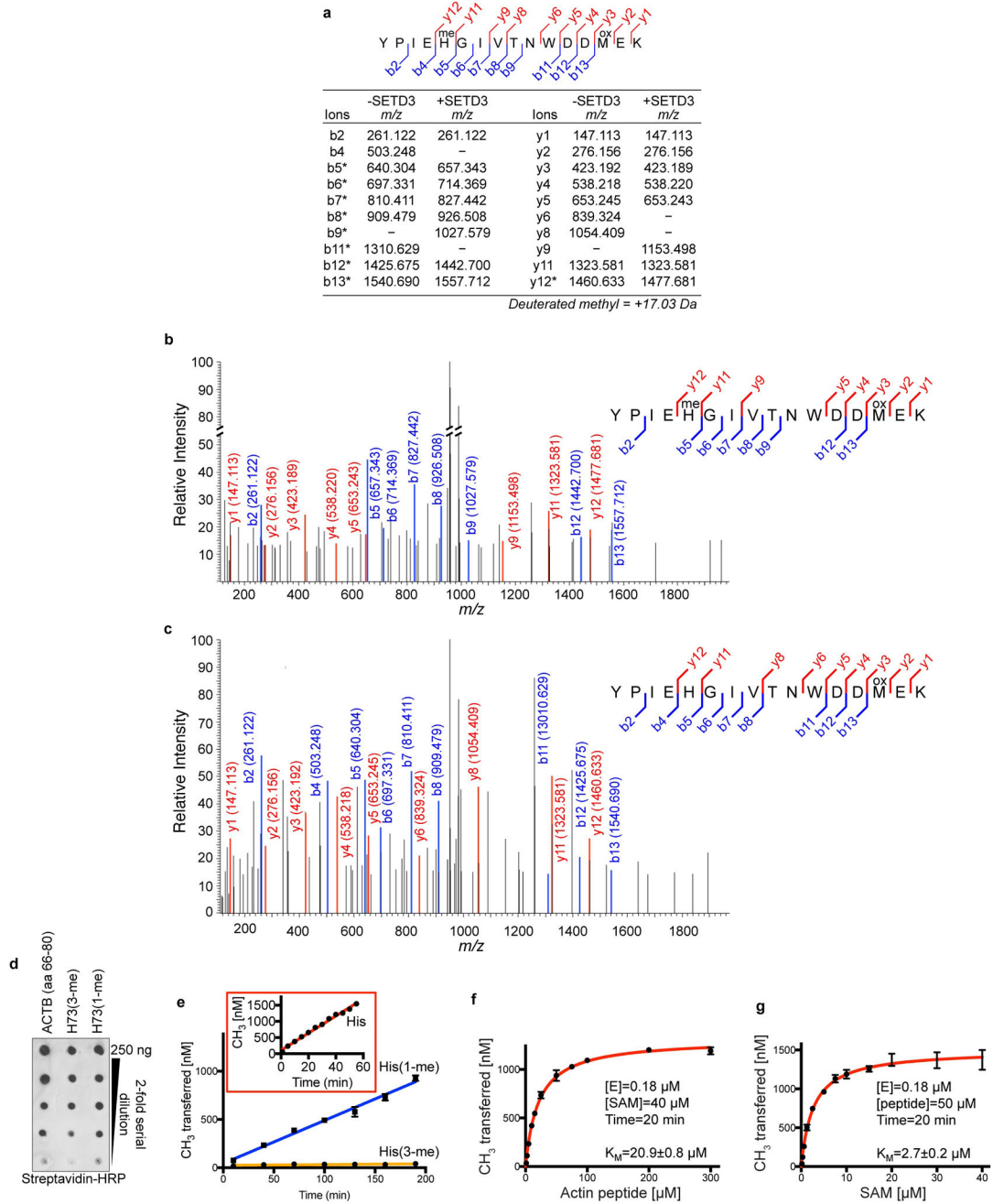
localization in HeLa cells (left) are merged with DAPI counterstaining (right). Scale bar, 7 μm. **d-g,** Biochemical enrichment of a candidate SETD3 substrate. **d,** Schematic of biochemical strategy to identify methylated band indicated in Fig. 1b. **e,** *in vitro* methylation reactions using cell extracts separated by size-exclusion chromatography as a substrate. Reactions were performed with either wild-type (WT) SETD3 or a putative catalytic mutant (Y312A). Reactions were analyzed as in Fig. 1. Arrowhead, candidate substrate. **f,** Ion-exchange chromatography separates candidate substrates. Fractions positive for SETD3-specific methylation by size-exclusion chromatography were further separated by ion-exchange chromatography and either the flowthrough (FT) or pooled fractions containing a significantly silver-stained band (arrowhead) at the size of the candidate substrate were used as substrate in an *in vitro* methylation reaction. **g,** Flowthrough (FT) or pooled eluent from ion-exchange chromatography were used as substrate for methylation reactions as in **e**. Arrowhead, protein band in eluent that was analyzed by mass spectrometry. **h,** Top candidate substrates with molecular weight (MW) similar to the size of SETD3-dependent band from *in vitro* reactions with cell extracts. Candidates identified by mass spectrometry are ranked by abundance determined by MS/MS count (Supplementary Table 1). **i,** *in vitro* methylation reactions with SETD3 on actin, recombinant histone H3 (rH3), FOXM1, or a no substrate as a control. Top panel, ^{3}H-SAM is the methyl donor and methylation visualized by autoradiography. Bottom panel, Coomassie staining of proteins in the reaction. **j,** *in vitro* methylation reactions with the indicated enzymes and substrates. All experiments were repeated at least three times with similar results.

Extended Data Figure 2. SETD3 does not methylate beta-actin lysines.
GST-beta-actin was expressed in bacteria, and cleaved using Prescission protease. Cleaved beta-actin was used in an *in vitro* methylation assay with SETD3 and deuterated SAM. Spectra are representative from experiments independently performed three times with similar results. MS/MS spectra with identified ions for unmethylated lysine residues produced with indicated proteases: **a,** K18 (trypsin) (Identified N-terminal GPLGS amino acids are residual, vector specific amino acids from the original GST fusion protein). **b,** K50 (trypsin); **c,** K61 (trypsin); **d,** K68 (trypsin)**; e,** K84 (chymotrypsin); **f,** K113 (trypsin); **g,** K118 (Glu-C); **h,** K191 (trypsin); **i,** K213 (trypsin); **j,** K215 (Glu-C)**; k,** K238
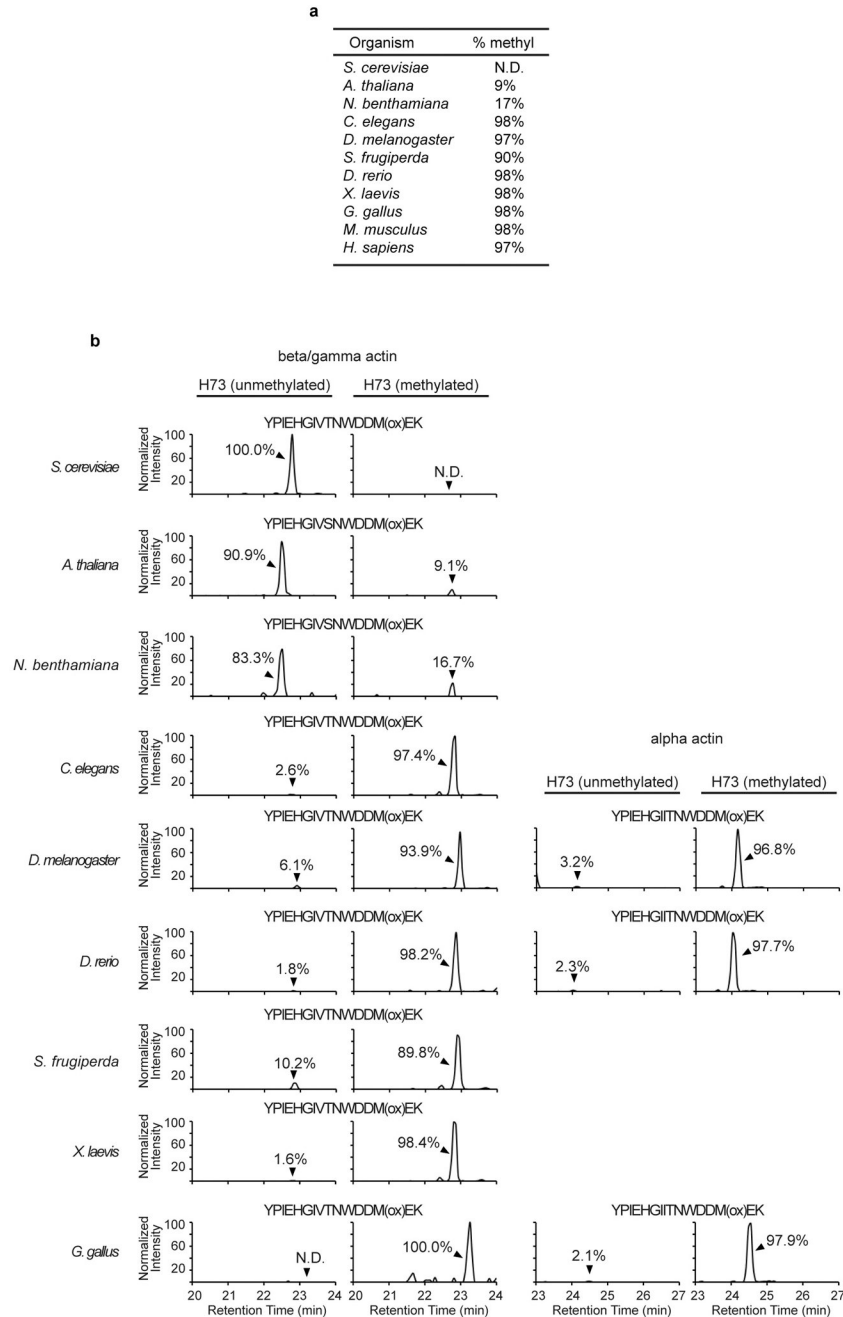
(chymotrypsin); **l,** K284/K291 (chymotrypsin); **m,** K315/K326 (trypsin); **n,** K326/K328 (trypsin); **o,** K336 (trypsin); **p,** K373 (trypsin).

a

Ions	-SETD3 m/z	+SETD3 m/z	Ions	-SETD3 m/z	+SETD3 m/z
b2	261.122	261.122	y1	147.113	147.113
b4	503.248	–	y2	276.156	276.156
b5*	640.304	657.343	y3	423.192	423.189
b6*	697.331	714.369	y4	538.218	538.220
b7*	810.411	827.442	y5	653.245	653.243
b8*	909.479	926.508	y6	839.324	–
b9*	–	1027.579	y8	1054.409	–
b11*	1310.629	–	y9	–	1153.498
b12*	1425.675	1442.700	y11	1323.581	1323.581
b13*	1540.690	1557.712	y12*	1460.633	1477.681

Deuterated methyl = +17.03 Da

Extended Data Figure 3. SETD3 generates actin-H73(3-me).

a-c, Tandem MS/MS identifies H73 of actin as SETD3 methylated residue. **a,** *Top:* Methylated tryptic peptide with indicated b and y ions. Modifications: me, methylation; ox, oxidation. *Bottom:* Table of *m/z* for b and y ions identified in MS/MS spectra from methylation reactions with (+SETD3) or without (-SETD3) using deuterated SAM as the methyl donor (+17.03 Da mass shift). *, peptides containing H73. **b-c**, *in vitro* methylation

reactions with (**b**) or without (**c**, negative control) SETD3 and beta-actin with deuterated *S*-adenosyl-methionione (SAM) were analyzed by mass spectrometry. *Left*, MS/MS spectra of tryptic peptides containing H73. *Right*, b and y ions identified of oxidized (ox) peptides in each spectrum are indicated. me, methylation. **d,** Dot blot loading control for Fig. 2c of biotinylated ACTB peptides (amino acids 66-80) that are unmodified at H73 or methylated in the *N*3 (3-me) or *N*1 (1-me) position. Serial dilutions of peptide were visualized by streptavidin-HRP and chemiluminescence. **e-g,** Methylation reaction kinetics for SETD3 and actin peptide. **e,** Time-course of SETD3 with His(1-me) or His(3-me) modified peptides as substrate. *Inset*: unmodified peptide using 80-fold lower enzyme concentration as that used for modified peptides. **f-g,** Steady-state kinetics of SETD3 for **f,** human beta-actin peptide (residues 66-80) and **g,** SAM. Kinetic measurements were performed using a bioluminescent methyltransferase assay, MTase-Glo™ (Promega). Means from biological triplicates for each data point are reported and error bars indicate standard deviation. **a-g,** Data are representative of three independent experiments with similar results.

a,

Organism	% methyl
S. cerevisiae	N.D.
A. thaliana	9%
N. benthamiana	17%
C. elegans	98%
D. melanogaster	97%
S. frugiperda	90%
D. rerio	98%
X. laevis	98%
G. gallus	98%
M. musculus	98%
H. sapiens	97%

Extended Data Figure 4. Methylation of the conserved actin-H73 residue is present in diverse organisms.

a, Summary of actin histidine methylation on the conserved H73 residue among model organisms. Abundance of methylation is reported as a percent of peptide that is methylated. **b,** Chromatograms for MH^{3+} ions ($m/z \pm 10$ ppm) for methylated and unmethylated versions of the indicated peptides. The unmethylated actin peptide that was analyzed for each species is shown above the corresponding chromatograms (ox, oxidation). When alpha-actin peptides were detected, associated chromatograms and quantification are provided on right. The area of indicated peaks was normalized to the sum area between peptides (±

methylation) and percent abundance is labeled. Chromatograms quantifying actin histidine methylation in human and mouse can be found in Extended Data Fig. 6 and 7. **a-b,** N.D., not detected. Quantification represents data from two independent experiments with similar results.
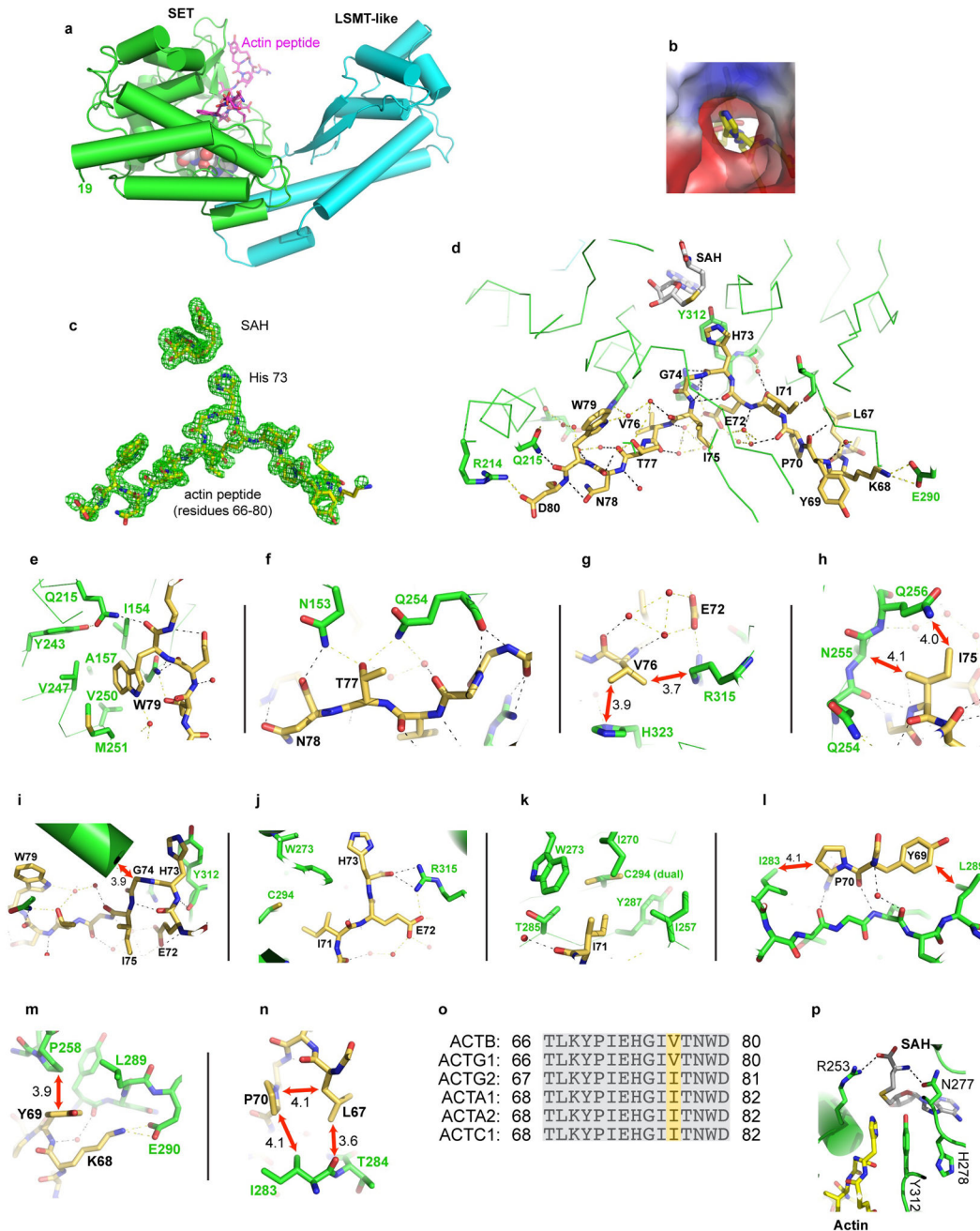
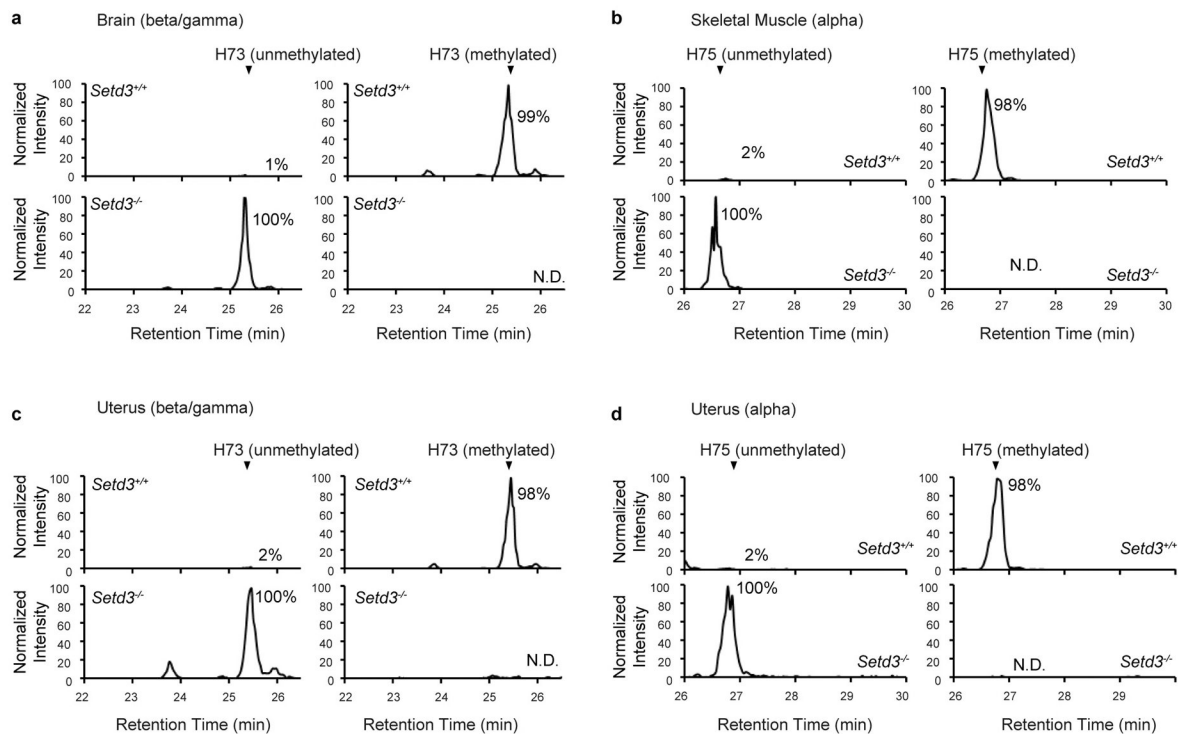**Extended Data Figure 5. Structural details of SETD3-actin peptide interactions.**
a, Overall structure of SETD3 with a V-shaped cleft constructed by the SET domain (green) and an LSMT-like domain (cyan). Helices are shown as cylinders and strands as arrows. Actin peptide shown as a stick model. **b,** View of the target histidine through

the channel from the SAH binding pocket. **c,** Omit electron density of Fo-Fc, contoured at 3.0σ above the mean, is shown for omitting cofactor SAH and the actin peptide used for co-crystallization. **d,** Details of inter- and intramolecular interactions between SETD3 (green) and actin peptide (yellow). **e,** W79 of actin bound in a hydrophobic surface pocket of SETD3. **f,** T77 and N78 of actin form hydrogen bonds with N153 and Q254 of SETD3. **g,** V76 of actin is in van der Waals contact with SETD3 residues H323 and R315, which in turn interacts with E72 of actin. **h,** I75 of actin is in van der Waals contact with main-chain Cα of N255 and Q256 of SETD3. **i,** G74 of actin is located in the amino end of a SETD3 helix. The imidazole ring of H73 (the substrate target) is parallel with the aromatic ring of Y312 of SETD3. **j,** SETD3 R315 bridges between the carboxylate oxygen of E72 and the main-chain carbonyl oxygen of H73 of actin. **k,** I71 of actin is accommodated in a surface hydrophobic pocket of SETD3. **l,** Y69 and P70 of actin interact with a stretch of SETD3 residues from I283 to L289. **m,** Y69 of actin packs against P258 of SETD3 and K68 of actin interacts with E290 of SETD3. **n,** L67 and P70 of actin form an intra-molecular interaction and both interact with I283 and T284 of SETD3. **o,** Alignment of the amino acids from all six human actin isoforms corresponding to beta-actin amino acids 66-80. Variant amino acid highlighted in yellow. **p,** The cofactor (SAH) binding site includes residues R253, Y312, N277 and H278 of SETD3.
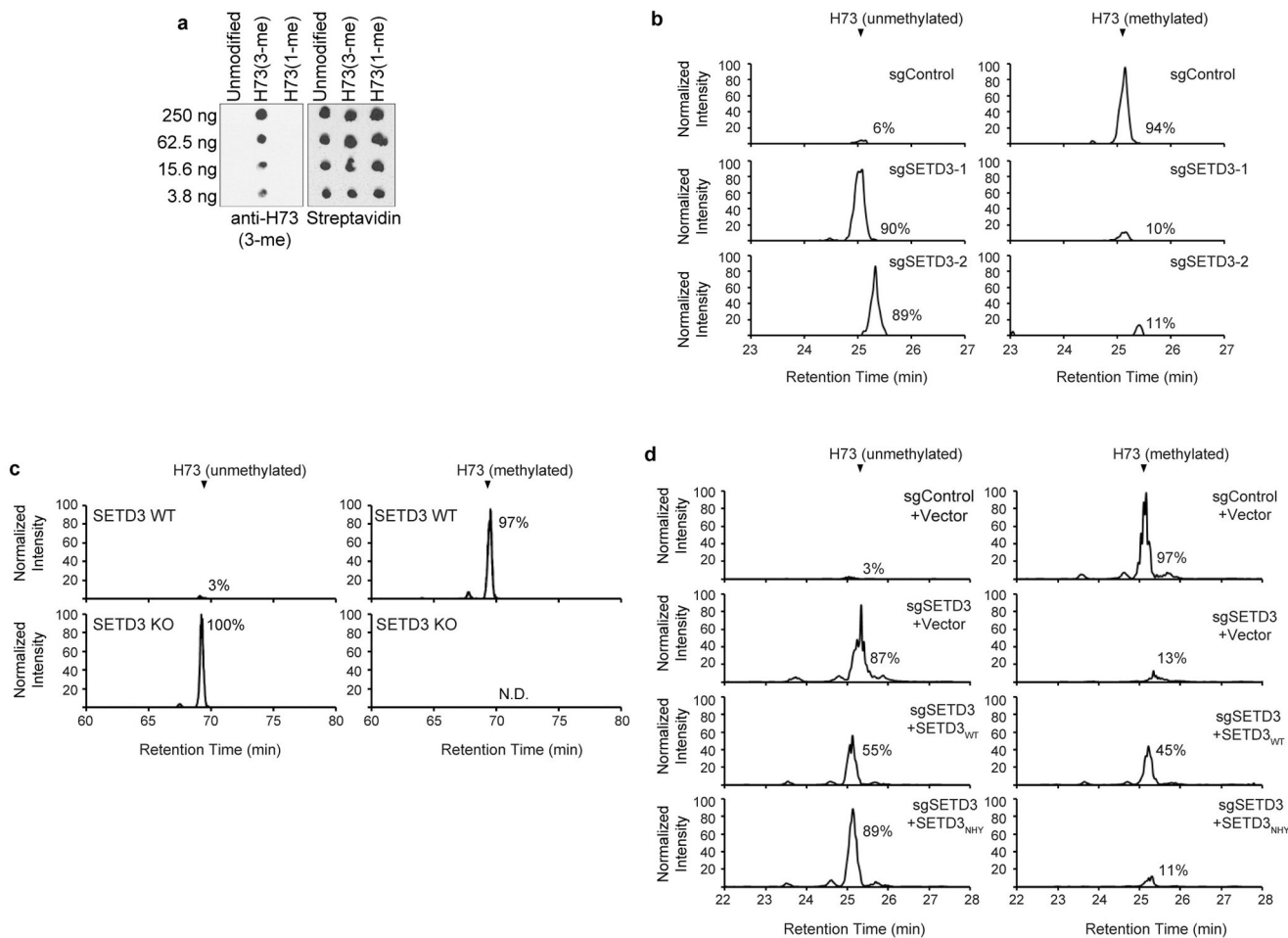
Extended Data Figure 6. SETD3 is required for actin methylation in cells.

a, Peptide dot blot spotted with biotinylated beta-actin peptides (amino acids 66-80) containing H73, H73(3-me), or H73(1-me). Blots were probed with H73(3-me)-specific antibody or streptavidin as a loading control. **b-d,** Chromatograms for quantification of actin-H73me in human cells. Stoichiometry of oxidized beta/gamma-actin H73 peptide (YPIEHGIVTNWDDM(ox)EK) with or without methylation after purification from cells. MH^{3+} m/z: unmethylated, 654.968 ± 10 ppm; methylated, 659.6401 ± 10 ppm. Alpha-actin peptide was not detected in these cells. Quantification performed as in Extended Data Fig. 4. **b,** Chromatograms for HT1080 cells treated with CRISPR/Cas9 that is targeted with a control sgRNA or SETD3-specific sgRNAs. **c,** Chromatograms for actin H73 methylation in wild-type (WT) HeLa cells or clonal HeLa SETD3 knockout (KO) cells. N.D., not detected. **d**, Chromatograms of actin H73 methylation in HT1080 cells treated with CRISPR/Cas9 targeted with a either a control or SETD3-specific sgRNA and complemented with CRISPR-resistant SETD3$_{WT}$, SETD3$_{NHY}$ or control plasmids. **a-d,** Experiments were performed three independent times with similar results.

a, Brain (beta/gamma)

b, Skeletal Muscle (alpha)

c, Uterus (beta/gamma)

d, Uterus (alpha)

e,

Amino Acid	Relative abundance KO/(WT+HET)
Histidine	0.935 ± 0.096
1-Methylhistidine	0.834 ± 0.104
3-Methylhistidine*	0.221 ± 0.076
Alanine	0.804 ± 0.183
Arginine	0.749 ± 0.106
Asparagine	0.867 ± 0.137
Aspartic Acid	0.785 ± 0.158
Glutamic Acid	0.861 ± 0.130
Glutamine	0.892 ± 0.065
Glycine	0.916 ± 0.072
Isoleucine	0.891 ± 0.136
Leucine	0.866 ± 0.142
Lysine	0.657 ± 0.210
Methionine	0.801 ± 0.143
Phenylalanine	1.002 ± 0.101
Proline	0.767 ± 0.187
Serine	0.871 ± 0.120
Threonine	0.821 ± 0.188
Tryptophan	0.799 ± 0.115
Tyrosine	0.991 ± 0.117
Valine	0.904 ± 0.118

Extended Data Figure 7. SETD3 is required for actin-H73 methylation in mice.
a-d, Chromatograms for quantification of actin histidine methylation in mouse tissues.
a, Chromatograms to determine abundance of histidine methylation from beta/gamma-actin H73 peptide (YPIEHGIVTNWDDM(ox)EK) with or without methylation after purification from brain tissue of mice with the indicated genotypes. MH^{3+} m/z: unmethylated, 654.968 ± 10 ppm; methylated, 659.640 ± 10 ppm. Alpha-actin peptide was not detected in these cells. Quantification performed as in Extended Data Fig. 4. **b,** Chromatograms to determine abundance of histidine methylation on alpha-actin H75 peptide (YPIEHGIITNWDDM(ox)EK) from skeletal muscle as in **a**. MH^{3+} m/z: unmethylated,

659.640 ± 10 ppm; methylated, 664.312 ± 10 ppm. Beta/gamma-actin peptide was not detected in these cells. **c,** Chromatograms to determine abundance of beta/gamma-actin H73 methylation from uterine tissue as in **a**. **d,** Chromatograms to determine abundance of alpha-actin H75 methylation from uterine tissue as in **b**. **a-d,** N.D., not detected. Quantification was performed three independent times with similar results. **e,** Table of quantitative amino acid panel from murine blood serum. Quantitative profiling of amino acids in plasma is used clinically to diagnose metabolic disorders. 3-methyl histidine (3MH) (indicated by asterisk) is one of the amino acids measured in the panel, and actin is thought to be the primary source of this metabolite. $Setd3^{-/-}$ (KO, $n = 8$) indicated amino acid levels were normalized to levels of amino acids from animals with normal H73 methylation levels (Total $n = 12$; $Setd3^{+/+}$ (WT), $n = 5$; $Setd3^{+/-}$ (HET), $n = 7$). Standard error of the difference between two means is shown for the indicated n.
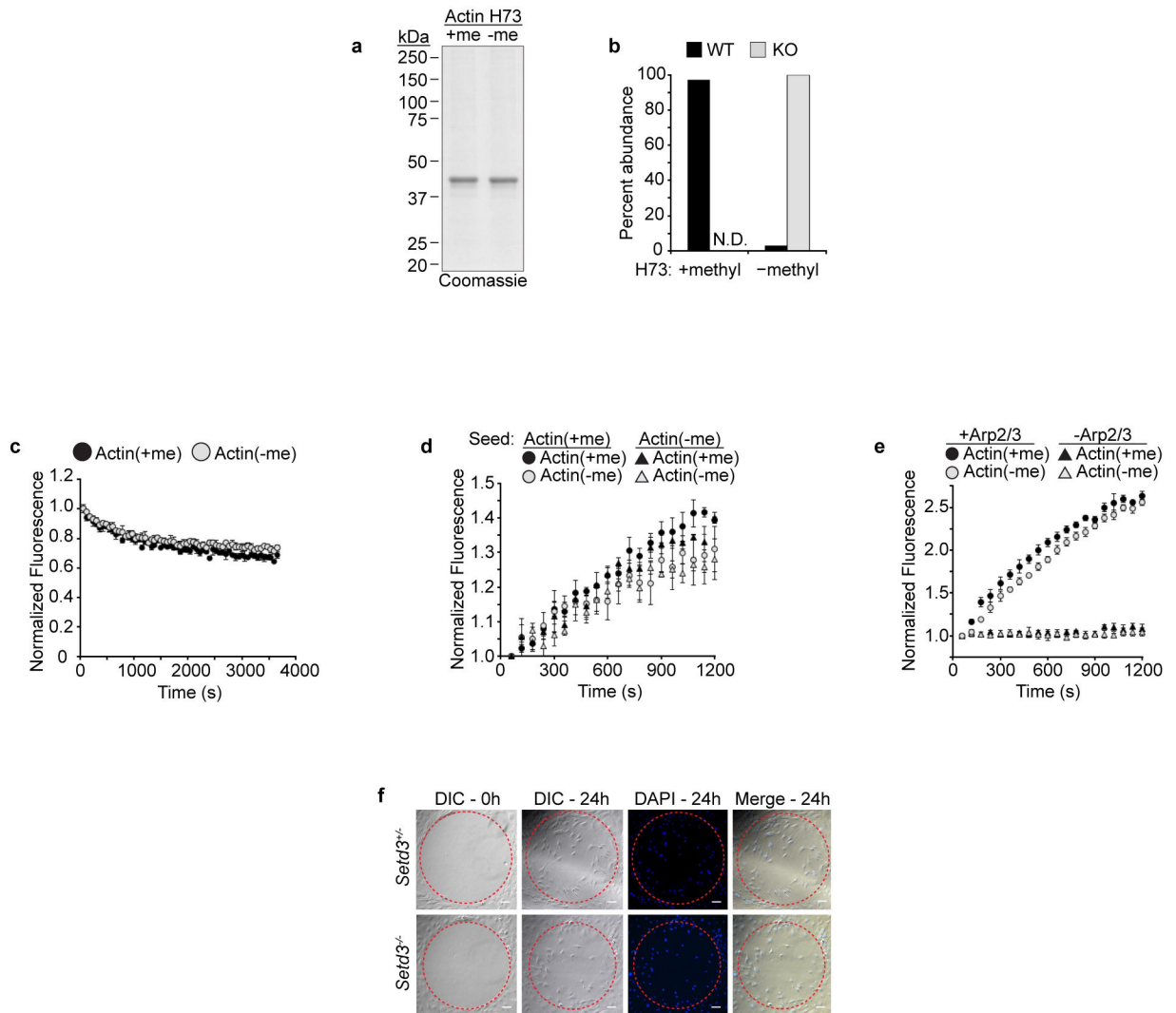
Extended Data Figure 8. SETD3-dependent actin-H73 methylation modestly regulates polymerization.

a-b, Purification of actin with and without H73 methylation. **a,** Coomassie stained gel of the actin purified from HeLa cell lines described in Fig. 3f, Actin(+me) or Actin(-me), and used in biochemical assays described in Fig. 4a-b and c-e. **b,** Mass spectrometry quantification of actin H73 methylation from **a**. N.D., not detected. **a-b,** Representative data from an experiment performed at least three times with similar results. **c,** Methylation does not alter actin depolymerization rates. Actin polymerized as in Fig. 4a was diluted to 0.02 μM and depolymerization was monitored by fluorescence normalized to initial values. **d,** Elongation of the indicated monomeric actin (1 μM, 0.1 μM pyrene-actin) measured in the presence of 2 μM phalloidin-actin seeds made with methylated (circles) or unmethylated (triangles). **e,** Arp2/3-induced actin polymerization performed in the presence of 100 nM WASP VCA and 5 nM Arp2/3 complex with 1 μM of the indicated monomeric actin and 0.1 μM pyrene-actin. **c-e,** Mean values plotted with s.e.m. from three independent biological replicates. **f,** SETD3 promotes cell migration. Representative images of cell migration assays performed three times with similar results using cells from Fig. 4c. A circular void of cells was created at the start of the assay (0h, dashed red circle). After 24h of migration, cells were fixed and stained with DAPI. Scale bar, 100 μm.
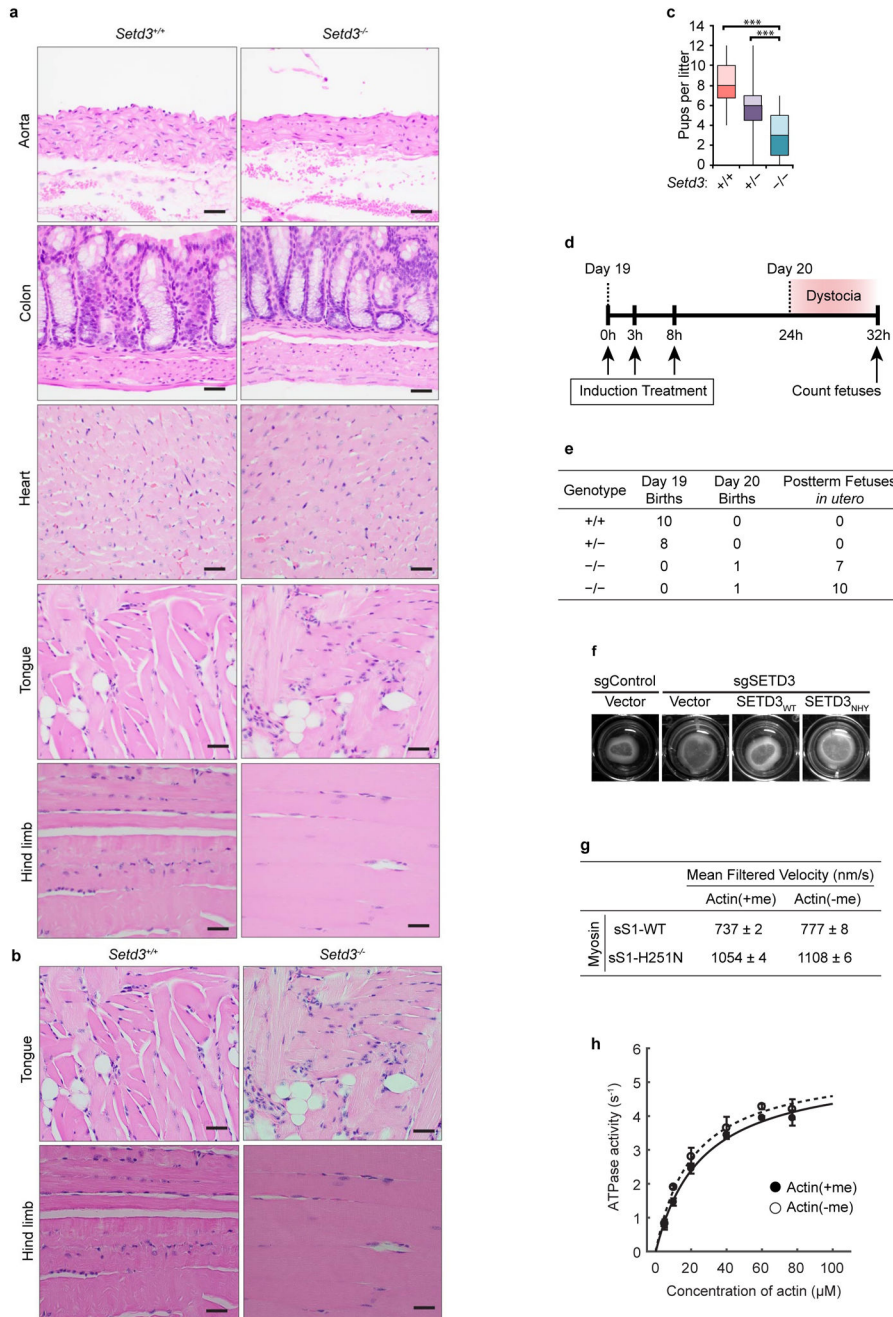
Extended Data Figure 9. Analysis of SETD3 and actin-H73me in parturition and uterine smooth muscle contraction.
a-b, Histology of muscle tissues from *Setd3*^{+/+} and *Setd3*^{−/−} mice. **a,** Hematoxylin and eosin staining of aorta, colon, heart, tongue, and hind limb muscle from *Setd3*^{+/+} and *Setd3*^{−/−} mice. **b,** Tongue and hind limb (striated muscle) sections from **a** were re-imaged without a condenser to highlight the sarcoplasmic striations characteristic of this muscle type. **a-b,** Scale bar: 20 μm. Images from three independent experiments gave similar results. **c,** Quantification of pups per litter for *Setd3*^{+/+} (*n* = 12), *Setd3*^{+/−} (*n* = 43), *Setd3*^{−/−} (*n* =26) mothers. ***, *p*-value = <0.001. **d-e,** Labor induction at 19 dpc does not rescue dystocia of

Setd3^{−/−} pregnant mice. **d,** Schematic of prostaglandin treatment protocol. PGF2α cocktail was administered at 0, 3, and 8 hours on day 19 with euthanasia and quantification of fetuses at 32h after first treatment. **e,** Table quantifying births and postterm fetuses *in utero* for the indicated genotypes at the time shown in the schematic. Note: controls delivered before treatment commenced. **f,** Collagen contraction assay as in Fig. 5h with indicated reconstitution cell lines from Fig. 5j performed with three independent biological replicates. **g-h,** Actin-H73me does not notably alter myosin activity. **g,** *in vitro* actin motility assay. Gliding velocities of actin filaments prepared from actin described in Fig. 4 were measured using human β-cardiac sS1 myosin or a hyperactive mutant (H251N). Data are mean velocities with s.e.m. from four different experiments. **h,** Actin-activated ATPase of human β-cardiac sS1 using actin as in **g**. The Michaelis-Menten equation is fit to the ATPase data for WT actin (solid line) and KO actin (dashed line). Points are means from two independent experiments. For gel source data, see Supplementary Fig. 1.

Extended Data Table 1.

Summary of X-ray data collection from SERCAT beamline (22-ID) at wavelength = 1Å and refinement statistics. (*)

SETD3	Actin peptide SAH	Actin peptide SAH	Actin peptide SAH
PDB Code	**6MBJ**	**6MBK**	**6MBL**
Data Collection			
Space group	$P2_1$	$P2_12_12_1$	$P2_12_12_1$
Cell dimensions (Å)	60.35, 176.17, 66.58	60.28, 115.97, 173.59	56.56, 92.83, 111.64
α, β, γ (°)	90, 92.9, 90	90, 90, 90	90, 90, 90
Resolution (Å)	39.07-1.79 (1.85-1.79)	39.38-1.69 (1.75-1.69)	48.30-2.19 (2.27-2.19)
[a] R_{merge}	0.146 (0.892)	0.129 (0.800)	0.125 (0.741)
R_{pim}	0.041 (0.436)	0.061 (0.592)	0.066 (0.548)
$CC_{1/2}$, CC	(0.463, 0.795)	(0.720, 0.915)	(0.402, 0.757)
[b] $<I/\sigma I>$	14.5 (1.0)	11.3 (1.7)	14.1 (1.5)
Completeness (%)	94.5 (78.9)	99.2 (98.4)	99.5 (96.7)
Redundancy	13.6 (8.0)	19.2 (8.9)	10.6 (4.7)
Observed reflections	1,695,347	2,597,462	323,060
Unique reflections	124,387 (10,380)	135,382 (13,262)	30,434 (2920)
Refinement			
Resolution (Å)	1.79	1.69	2.19
No. reflections	123,743	135,110	30,334
[c] R_{work} / [d] R_{free}	0.199 / 0.223	0.228 / 0.243	0.182 / 0.227
No. Atoms	Two complexes	Two complexes	One complex
Protein	7824	7953	3923
Peptide	248	252	124
SAH	52	52	26
Solvent	777	933	179
B-factors (Å²)			

SETD3	Actin peptide SAH	Actin peptide SAH	Actin peptide SAH
PDB Code	**6MBJ**	**6MBK**	**6MBL**
Protein	34.3	29.6	47.3
Peptide	41.4	34.5	42.3
SAH	18.0	16.7	32.0
Solvent	45.2	39.9	46.5
R.m.s. deviations			
Bond lengths (Å)	0.003	0.010	0.004
Bond angles (°)	0.564	0.942	0.683

Values in parenthesis correspond to highest resolution shell.

[a], $R_{merge} = \Sigma \mid I - <I> \mid / \Sigma I$, where I is the observed intensity and <I> is the averaged intensity from multiple observations.

[b], $<I/\sigma I>$ = averaged ratio of the intensity (I) to the error of the intensity (σI).

[c], $R_{work} = \Sigma \mid Fobs - Fcal \mid / \Sigma \mid Fobs \mid$, where Fobs and Fcal are the observed and calculated structure factors, respectively.

[d], R_{free} was calculated using a randomly chosen subset (5%) of the reflections not used in refinement.

Supplementary Material

Refer to Web version on PubMed Central for supplementary material.

Acknowledgements

References

1. Johnson P, Harris CI & Perry SV 3-methylhistidine in actin and other muscle proteins. Biochem J 103, 79P (1967). [PubMed: 6033776]

2. Seaborne RA et al. Human Skeletal Muscle Possesses an Epigenetic Memory of Hypertrophy. Sci Rep 8, 1898, doi:10.1038/s41598-018-20287-3 (2018). [PubMed: 29382913]

3. Carlson SM & Gozani O Nonhistone Lysine Methylation in the Regulation of Cancer Pathways. Cold Spring Harb Perspect Med 6, doi:10.1101/cshperspect.a026435 (2016).

4. Eom GH et al. Histone methyltransferase SETD3 regulates muscle differentiation. J Biol Chem 286, 34733–34742, doi:10.1074/jbc.M110.203307 (2011). [PubMed: 21832073]

5. Chang Y et al. Structural basis of SETD6-mediated regulation of the NF-kB network via methyl-lysine signaling. Nucleic Acids Res 39, 6380–6389, doi:10.1093/nar/gkr256 (2011). [PubMed: 21515635]

6. Levy D et al. Lysine methylation of the NF-kappaB subunit RelA by SETD6 couples activity of the histone methyltransferase GLP at chromatin to tonic repression of NF-kappaB signaling. Nat Immunol 12, 29–36, doi:ni.1968 [pii]10.1038/ni.1968 (2011). [PubMed: 21131967]

7. Clarke SG Protein methylation at the surface and buried deep: thinking outside the histone box. Trends Biochem Sci 38, 243–252, doi:10.1016/j.tibs.2013.02.004 (2013). [PubMed: 23490039]

8. Webb KJ et al. A novel 3-methylhistidine modification of yeast ribosomal protein Rpl3 is dependent upon the YIL110W methyltransferase. J Biol Chem 285, 37598–37606, doi:10.1074/jbc.M110.170787 (2010). [PubMed: 20864530]

9. Kalhor HR et al. A highly conserved 3-methylhistidine modification is absent in yeast actin. Arch Biochem Biophys 370, 105–111, doi:10.1006/abbi.1999.1370 (1999). [PubMed: 10496983]

10. Schubert HL, Blumenthal RM & Cheng X Many paths to methyltransfer: a chronicle of convergence. Trends Biochem Sci 28, 329–335, doi:10.1016/S0968-0004(03)00090-2 (2003). [PubMed: 12826405]

11. Del Rizzo PA & Trievel RC Substrate and product specificities of SET domain methyltransferases. Epigenetics 6, 1059–1067, doi:10.4161/epi.6.9.16069 (2011). [PubMed: 21847010]

12. Yao X, Grade S, Wriggers W & Rubenstein PA His(73), often methylated, is an important structural determinant for actin. A mutagenic analysis of HIS(73) of yeast actin. J Biol Chem 274, 37443–37449 (1999). [PubMed: 10601317]

13. Dickinson ME et al. High-throughput discovery of novel developmental phenotypes. Nature 537, 508–514, doi:10.1038/nature19356 (2016). [PubMed: 27626380]

14. Nyman T et al. The role of MeH73 in actin polymerization and ATP hydrolysis. J Mol Biol 317, 577–589, doi:10.1006/jmbi.2002.5436 (2002). [PubMed: 11955010]

15. Narver HL Oxytocin in the treatment of dystocia in mice. J Am Assoc Lab Anim Sci 51, 10–17 (2012). [PubMed: 22330862]

16. Smith R, Imtiaz M, Banney D, Paul JW & Young RC Why the heart is like an orchestra and the uterus is like a soccer crowd. Am J Obstet Gynecol 213, 181–185, doi:10.1016/j.ajog.2015.06.040 (2015). [PubMed: 26116101]

17. Guo DC et al. Mutations in smooth muscle alpha-actin (ACTA2) cause coronary artery disease, stroke, and Moyamoya disease, along with thoracic aortic disease. Am J Hum Genet 84, 617–627, doi:10.1016/j.ajhg.2009.04.007 (2009). [PubMed: 19409525]

18. Milewicz DM et al. De novo ACTA2 mutation causes a novel syndrome of multisystemic smooth muscle dysfunction. Am J Med Genet A 152A, 2437–2443, doi:10.1002/ajmg.a.33657 (2010). [PubMed: 20734336]

19. Cao XJ, Arnaudo AM & Garcia BA Large-scale global identification of protein lysine methylation in vivo. Epigenetics 8, 477–485, doi:10.4161/epi.24547 (2013). [PubMed: 23644510]

20. Cooper K & Brown S ACTA2 mutation and postpartum hemorrhage: a case report. BMC Med Genet 18, 143, doi:10.1186/s12881-017-0505-5 (2017). [PubMed: 29202781]

21. Gunst SJ & Zhang W Actin cytoskeletal dynamics in smooth muscle: a new paradigm for the regulation of smooth muscle contraction. Am J Physiol Cell Physiol 295, C576–587, doi:10.1152/ajpcell.00253.2008 (2008). [PubMed: 18596210]

22. Rothbart SB, Krajewski K, Strahl BD & Fuchs SM Peptide microarrays to interrogate the "histone code". Methods in enzymology 512, 107–135, doi:10.1016/b978-0-12-391940-3.00006-8 (2012). [PubMed: 22910205]

23. Patel A, Dharmarajan V, Vought VE & Cosgrove MS On the mechanism of multiple lysine methylation by the human mixed lineage leukemia protein-1 (MLL1) core complex. The Journal of biological chemistry 284, 24242–24256, doi:10.1074/jbc.M109.014498 (2009). [PubMed: 19556245]

24. Edmunds JW, Mahadevan LC & Clayton AL Dynamic histone H3 methylation during gene induction: HYPB/Setd2 mediates all H3K36 trimethylation. The EMBO journal 27, 406–420, doi:10.1038/sj.emboj.7601967 (2008). [PubMed: 18157086]

25. An S, Yeo KJ, Jeon YH & Song JJ Crystal structure of the human histone methyltransferase ASH1L catalytic domain and its implications for the regulatory mechanism. The Journal of biological chemistry 286, 8369–8374, doi:10.1074/jbc.M110.203380 (2011). [PubMed: 21239497]

26. Chuikov S et al. Regulation of p53 activity through lysine methylation. Nature 432, 353–360, doi:10.1038/nature03117 (2004). [PubMed: 15525938]

27. Feng Q et al. Methylation of H3-lysine 79 is mediated by a new family of HMTases without a SET domain. Current biology : CB 12, 1052–1058 (2002). [PubMed: 12123582]

28. Huang J et al. Repression of p53 activity by Smyd2-mediated methylation. Nature 444, 629–632, doi:10.1038/nature05287 (2006). [PubMed: 17108971]

29. Rea S et al. Regulation of chromatin structure by site-specific histone H3 methyltransferases. Nature 406, 593–599, doi:10.1038/35020506 (2000). [PubMed: 10949293]

30. Tachibana M, Sugimoto K, Fukushima T & Shinkai Y Set domain-containing protein, G9a, is a novel lysine-preferring mammalian histone methyltransferase with hyperactivity and specific selectivity to lysines 9 and 27 of histone H3. The Journal of biological chemistry 276, 25309–25317, doi:10.1074/jbc.M101914200 (2001). [PubMed: 11316813]

31. Kuo AJ et al. NSD2 links dimethylation of histone H3 at lysine 36 to oncogenic programming. Molecular cell 44, 609–620, doi:10.1016/j.molcel.2011.08.042 (2011). [PubMed: 22099308]

32. Mazur PK et al. SMYD3 links lysine methylation of MAP3K2 to Ras-driven cancer. Nature 510, 283–287, doi:10.1038/nature13320 (2014). [PubMed: 24847881]

33. Fang J et al. Purification and functional characterization of SET8, a nucleosomal histone H4-lysine 20-specific methyltransferase. Current biology : CB 12, 1086–1099 (2002). [PubMed: 12121615]

34. Kurash JK et al. Methylation of p53 by Set7/9 mediates p53 acetylation and activity in vivo. Molecular cell 29, 392–400, doi:10.1016/j.molcel.2007.12.025 (2008). [PubMed: 18280244]

35. Levy D et al. Lysine methylation of the NF-kappaB subunit RelA by SETD6 couples activity of the histone methyltransferase GLP at chromatin to tonic repression of NF-kappaB signaling. Nature immunology 12, 29–36, doi:10.1038/ni.1968 (2011). [PubMed: 21131967]

36. Baymaz HI, Spruijt CG & Vermeulen M Identifying nuclear protein-protein interactions using GFP affinity purification and SILAC-based quantitative mass spectrometry. Methods in molecular biology (Clifton, N.J.) 1188, 207–226, doi:10.1007/978-1-4939-1142-4_15 (2014).

37. Hsiao K, Zegzouti H & Goueli SA Methyltransferase-Glo: a universal, bioluminescent and homogenous assay for monitoring all classes of methyltransferases. Epigenomics 8, 321–339, doi:10.2217/epi.15.113 (2016). [PubMed: 26950288]

38. Cox J & Mann M MaxQuant enables high peptide identification rates, individualized p.p.b.-range mass accuracies and proteome-wide protein quantification. Nature biotechnology 26, 1367–1372, doi:10.1038/nbt.1511 (2008).

39. Kron SJ, Drubin DG, Botstein D & Spudich JA Yeast actin filaments display ATP-dependent sliding movement over surfaces coated with rabbit muscle myosin. Proceedings of the National Academy of Sciences of the United States of America 89, 4466–4470 (1992). [PubMed: 1533933]

40. Schafer DA, Jennings PB & Cooper JA Rapid and efficient purification of actin from nonmuscle sources. Cell motility and the cytoskeleton 39, 166–171, doi:10.1002/(sici)1097-0169(1998)39:2<166::aid-cm7>3.0.co;2-4 (1998). [PubMed: 9484958]

41. Otwinowski Z, Borek D, Majewski W & Minor W Multiparametric scaling of diffraction intensities. Acta crystallographica. Section A, Foundations of crystallography 59, 228–234 (2003). [PubMed: 12714773]

42. McCoy AJ et al. Phaser crystallographic software. Journal of applied crystallography 40, 658–674, doi:10.1107/s0021889807021206 (2007). [PubMed: 19461840]

43. Afonine PV et al. Towards automated crystallographic structure refinement with phenix.refine. Acta crystallographica. Section D, Biological crystallography 68, 352–367, doi:10.1107/s0907444912001308 (2012). [PubMed: 22505256]

44. Emsley P & Cowtan K Coot: model-building tools for molecular graphics. Acta crystallographica. Section D, Biological crystallography 60, 2126–2132, doi:10.1107/s0907444904019158 (2004). [PubMed: 15572765]

45. Hansen SD, Zuchero JB & Mullins RD Cytoplasmic actin: purification and single molecule assembly assays. Methods in molecular biology (Clifton, N.J.) 1046, 145–170, doi:10.1007/978-1-62703-538-5_9 (2013).

46. Yao X, Nguyen V, Wriggers W & Rubenstein PA Regulation of yeast actin behavior by interaction of charged residues across the interdomain cleft. The Journal of biological chemistry 277, 22875–22882, doi:10.1074/jbc.M201685200 (2002). [PubMed: 11940592]

47. Bradley A et al. The mammalian gene function resource: the International Knockout Mouse Consortium. Mammalian genome : official journal of the International Mammalian Genome Society 23, 580–586, doi:10.1007/s00335-012-9422-2 (2012). [PubMed: 22968824]

48. Le A, Ng A, Kwan T, Cusmano-Ozog K & Cowan TM A rapid, sensitive method for quantitative analysis of underivatized amino acids by liquid chromatography-tandem mass spectrometry (LC-MS/MS). Journal of chromatography. B, Analytical technologies in the biomedical and life sciences 944, 166–174, doi:10.1016/j.jchromb.2013.11.017 (2014). [PubMed: 24316529]

49. Adhikari AS et al. Early-Onset Hypertrophic Cardiomyopathy Mutations Significantly Increase the Velocity, Force, and Actin-Activated ATPase Activity of Human beta-Cardiac Myosin. Cell reports 17, 2857–2864, doi:10.1016/j.celrep.2016.11.040 (2016). [PubMed: 27974200]

50. Sommese RF et al. Molecular consequences of the R453C hypertrophic cardiomyopathy mutation on human beta-cardiac myosin motor function. Proceedings of the National Academy of Sciences of the United States of America 110, 12607–12612, doi:10.1073/pnas.1309493110 (2013). [PubMed: 23798412]

51. Liu C, Kawana M, Song D, Ruppel KM & Spudich JA Controlling load-dependent kinetics of beta-cardiac myosin at the single-molecule level. 25, 505–514, doi:10.1038/s41594-018-0069-x (2018).

52. Kron SJ, Toyoshima YY, Uyeda TQ & Spudich JA Assays for actin sliding movement over myosin-coated surfaces. Methods in enzymology 196, 399–416 (1991). [PubMed: 2034132]

53. Nag S et al. Contractility parameters of human beta-cardiac myosin with the hypertrophic cardiomyopathy mutation R403Q show loss of motor function. Science advances 1, e1500511, doi:10.1126/sciadv.1500511 (2015). [PubMed: 26601291]

54. Kawana M, Sarkar SS & Sutton S Biophysical properties of human beta-cardiac myosin with converter mutations that cause hypertrophic cardiomyopathy. 3, e1601959, doi:10.1126/sciadv.1601959 (2017).

55. Mortensen KI, Sung J, Flyvbjerg H & Spudich JA Optimized measurements of separations and angles between intra-molecular fluorescent markers. Nature communications 6, 8621, doi:10.1038/ncomms9621 (2015).

56. Aksel T, Choe Yu E, Sutton S, Ruppel KM & Spudich JA Ensemble force changes that result from human cardiac myosin mutations and a small-molecule effector. Cell reports 11, 910–920, doi:10.1016/j.celrep.2015.04.006 (2015). [PubMed: 25937279]

57. Trybus KM Biochemical studies of myosin. Methods (San Diego, Calif.) 22, 327–335, doi:10.1006/meth.2000.1085 (2000).
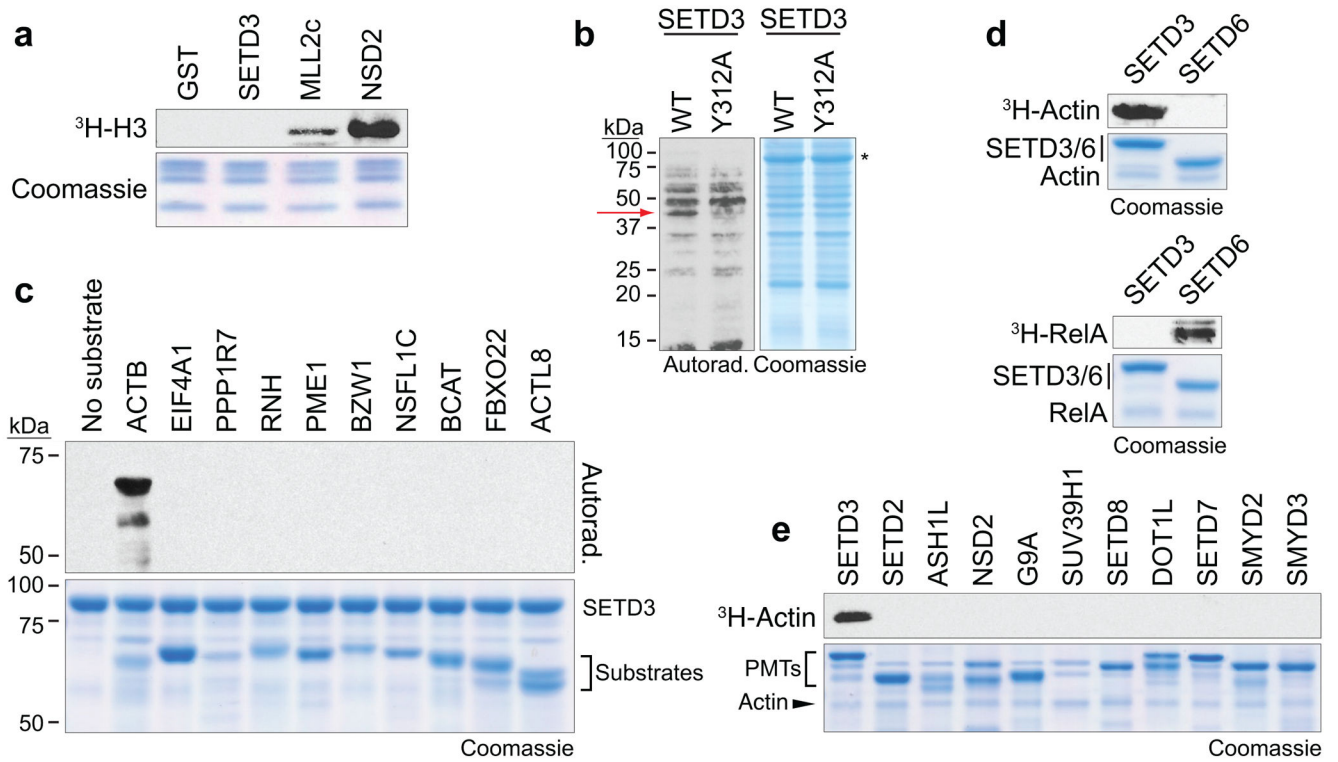
Figure 1. SETD3 specifically methylates actin.

a, SETD3 does not methylate histones. *in vitro* methylation reactions on recombinant nucleosomes with recombinant SETD3, minimal MLL2 catalytic complex (MLL2c), catalytically active NSD2 SET domain, or glutathione-*S*-transferase (GST) as a control. Top panel, ^{3}H-SAM is the methyl donor and methylation visualized by autoradiography. Bottom panel, Coomassie stain of nucleosomes used in the reaction. **b,** SETD3 methylates a cytoplasmic protein. *in vitro* methylation reactions as in **a** with recombinant SETD3 or a putative catalytic mutant (Y312A) on cytoplasmic HT1080 cellular extracts as substrate. Red arrow, candidate substrate. *, SETD3. **c,** Actin is selectively methylated by SETD3. Methylation assays as in **a** with SETD3 and the indicated recombinant candidate substrates. **d,** Methylation assays with SETD3 and SETD6 on actin and RelA. **e,** Methylation assays with the indicated SET domain PKMTs using recombinant beta-actin as a substrate. Experiments were independently performed 3 times with similar results. For gel source data, see Supplementary Fig. 1.
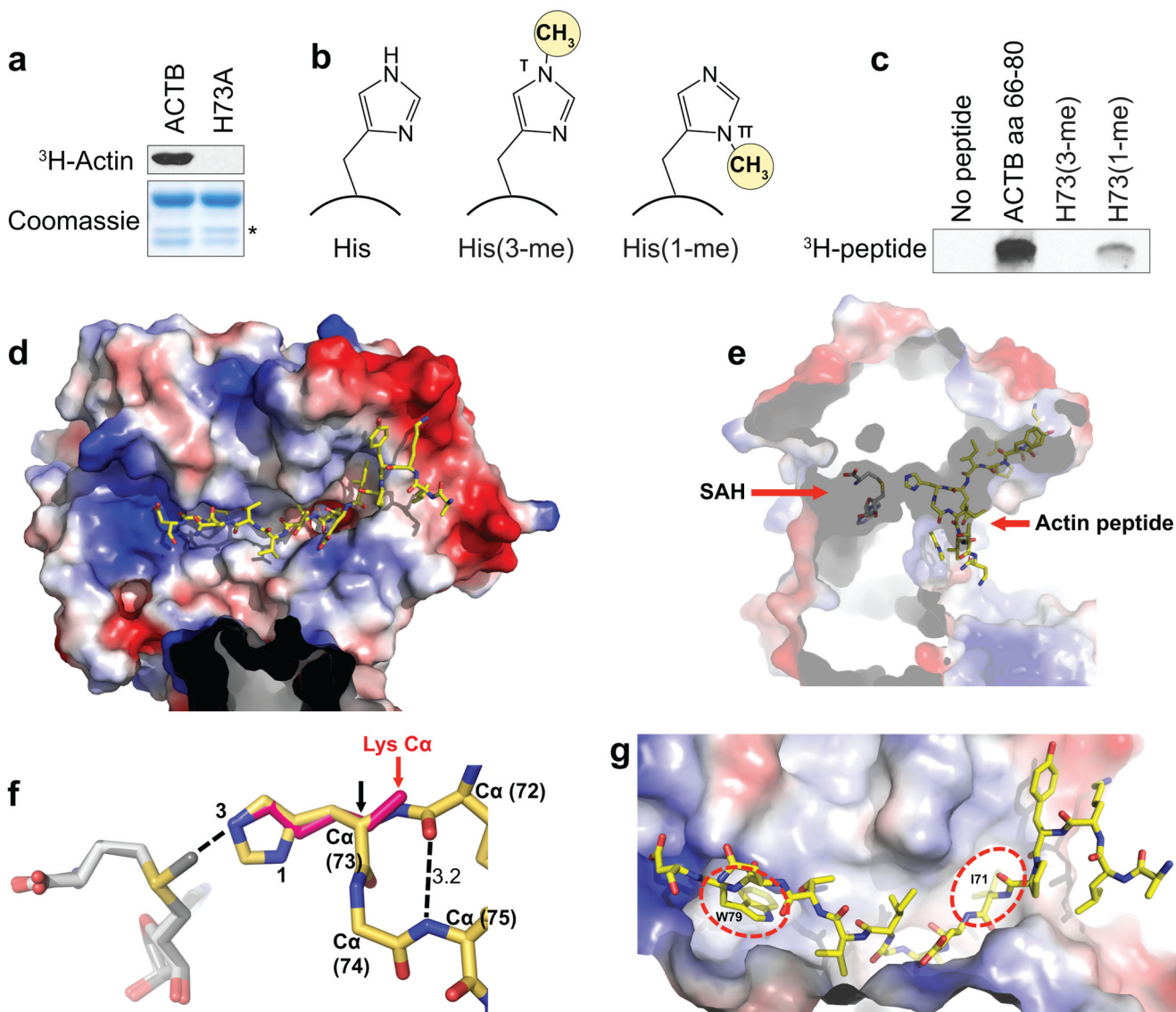
Figure 2. SETD3 methylates actin at histidine 73.

a, *in vitro* methylation assay with recombinant wild-type beta-actin or H73A mutant. *, non-specific bacterial contaminant. **b,** Histidine methylation: left, histidine; center, 3-(τ)-methyl histidine; right, 1-(π)-methyl histidine. **c,** SETD3 generates H73(3-me). *in vitro* methylation reactions with SETD3 on the indicated peptides visualized by autoradiography. **a,c,** Experiments were independently performed three times with similar results. **d-h,** The molecular basis for SETD3 recognition of actin. **d,** A long surface groove of the SET domain accommodates the actin peptide (stick model). Surface is colored blue for positive, red for negative, and white for neutral charges. **e,** A cut-through view of the SET domain illustrates cofactor SAH and actin peptide approaching from opposing faces and meeting in the middle of the active-site channel. **f,** A superimposition of SETD6 (showing the SAM and target lysine residue in magenta) and SETD3 bound with actin peptide showing residues immediately before and after His73. **g,** Close-up view of actin peptide binding groove with

side chains W79 and I71 inserted into two hydrophobic pockets (circled in red dashed lines). For gel source data, see Supplementary Fig. 1.
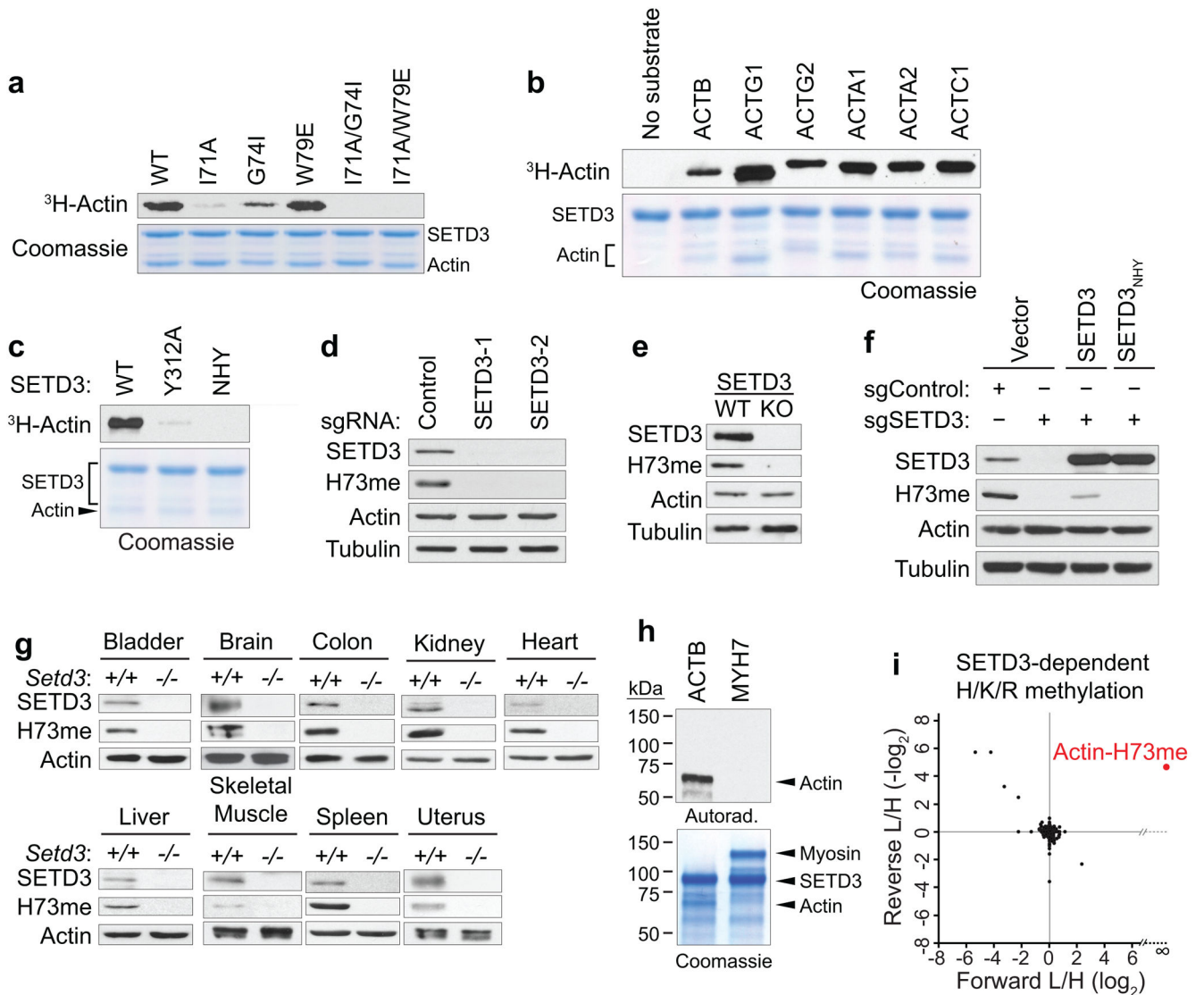
Author Manuscript

Figure 3. SETD3 is the principal enzyme generating actin-H73me in cells and *in vivo*.
a, *in vitro* methylation assay with SETD3 on indicated structure-guided actin mutants.
b, SETD3 methylation reactions on all human actin isoforms. **c,** Analysis of methylation
activity of SETD3 mutants: Y312A, catalytic tyrosine; NHY, SAM-binding amino acids
(N277A/H278A) + Y312A. **d-e,** SETD3 is necessary for H73 methylation in cells.
d, Western blots with the indicated antibodies on HT1080 whole cell extracts (WCE)
expressing CRISPR/Cas9 and two independent single guide RNAs (sgRNAs) targeting
SETD3 or a control sgRNA. Actin levels do not change and tubulin is shown as a
loading control. **e,** Western blots probing WCE made from HeLa cells or a clonal SETD3
knockout. **f,** Western blots of SETD3-deficient HT1080 cells as in **e** complemented with
CRISPR-resistant SETD3$_{WT}$, SETD3$_{NHY}$ or control plasmids. **g,** SETD3 mediates actin
H73 methylation *in vivo*. Whole tissue extracts were made from the indicated tissues
from *Setd3$^{+/+}$* and *Setd3$^{-/-}$* mice and analyzed by Western blot. **h,** *in vitro* reactions
with SETD3 and SETD6 on purified beta-cardiac myosin sS1 (MYH7) and beta-actin as

a positive control. **i,** Methylation of actin-H73 is the only change out of >900 lysine, arginine, and histidine methylation events detected upon SETD3 depletion in cells. SILAC-based quantitative proteomic analysis of methylated peptides in cells ±SETD3 using HeLa cells from **e**. SILAC ratios from two independent experiments are plotted in the forward direction (x-axis, $\log_2$-transformed) and the label-swapped reverse direction (y-axis, $-\log_2$-transformed). Forward: WT, light; SETD3 KO, heavy. Reverse: WT, heavy; SETD3 KO, light. SETD3-dependent methylation events are found in the top-right quadrant. For actin-H73me, no heavy peptide was found in the forward direction due to complete loss of SETD3, so the ratio divisible by zero was plotted as infinite. An actin-H73me ratio is calculated in the reverse direction due to incomplete heavy amino acid labeling cross contamination. Experiments were independently performed three times with similar results. For gel source data, see Supplementary Fig. 1.
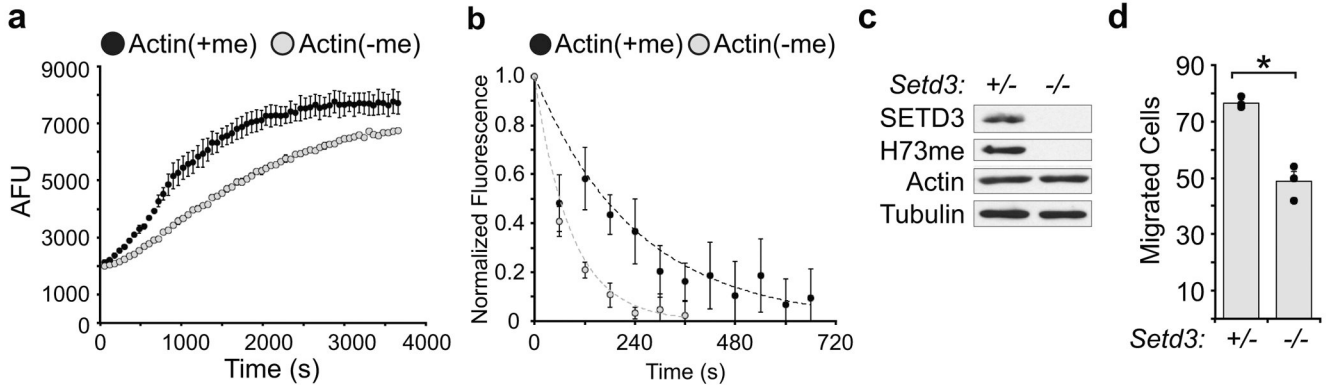
Figure 4. H73 methylation regulates actin behavior.
a-b,. Methylation increases actin polymerization. **a,** Pyrene-labeled skeletal muscle actin was added to the indicated actin in a 1:10 ratio (pyrene:Hela actin) and polymerization was monitored by arbitrary fluorescence units (AFU) with 5 μM actin. **b,** ATP exchange rates decrease due to H73 methylation. Actin saturated with ε-ATP was monitored for exchange with normal ATP by loss of fluorescence over time. Exponential curves (dashed lines) were drawn to the data by least squares fitting. **c-d,** SETD3 promotes cell migration. **c,** Western blot analysis of whole cell extracts from mouse embryonic fibroblasts isolated from *Setd3*^{+/−} and *Setd3*^{−/−} mice. **d,** Quantification of cell migration assays (see methods) over a 24h period. *, *p*-value = 0.002; unpaired two-tailed student's t-test. **a-d,** Graphs indicate the mean and s.e.m. from three independent biological replicates. All experiments independently repeated three times with similar results. For gel source data, see Supplementary Fig. 1.
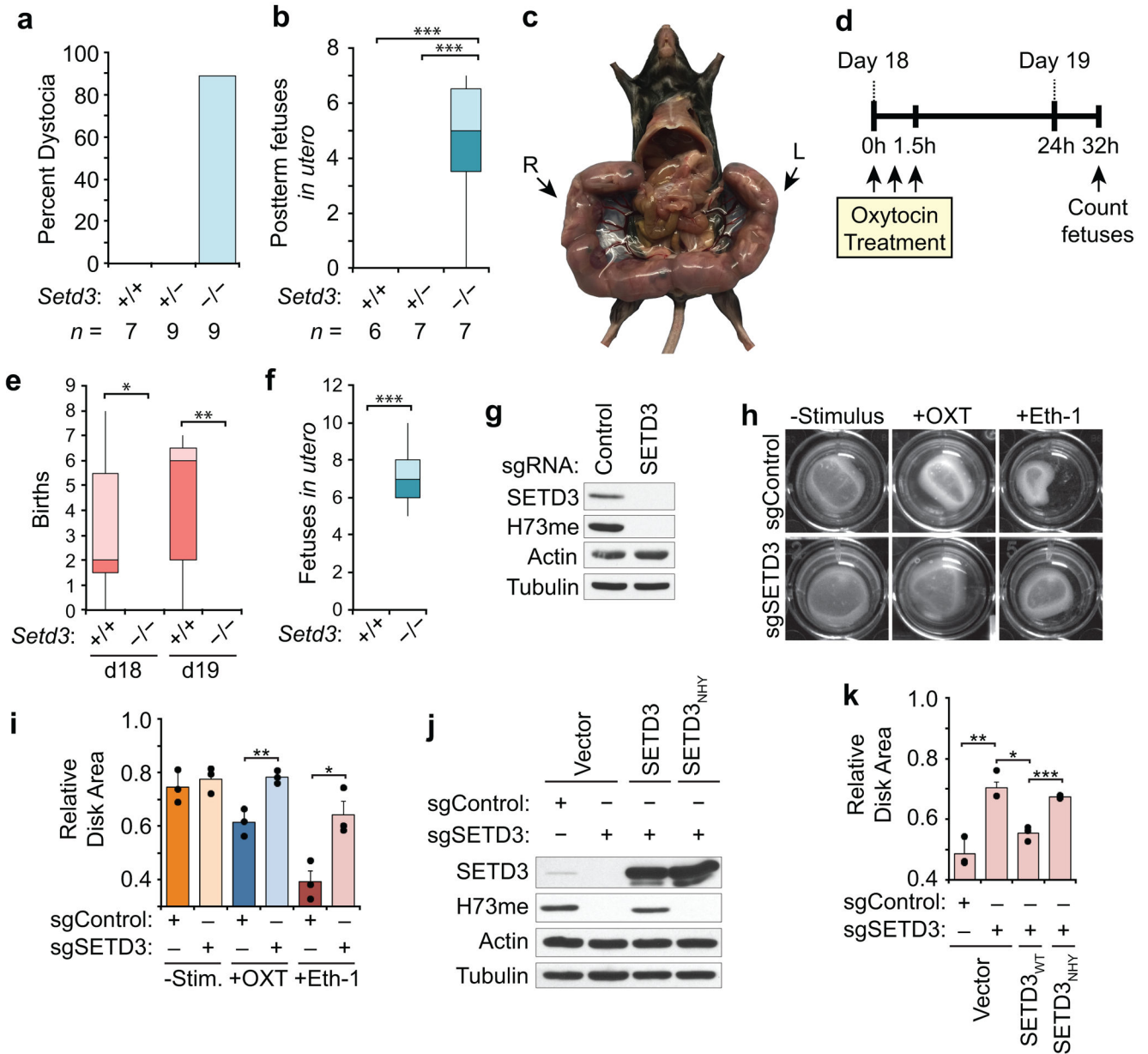
Figure 5. SETD3 regulates signal-induced smooth muscle contraction.

a-f, Primary dystocia in SETD3 deficient female mice. **a,** Percent of pregnant females with dystocia. Genotypes and *n* as noted. **b,** Fetuses remaining *in utero* were quantified at 20 dpc or 24h after giving birth for the indicated genotype. ***, *p*-value < 0.0001 from one-way ANOVA with Tukey's multiple comparison test. **c,** Example of a *Setd3*$^{-/-}$ female 20 dpc from **b** that had not given birth to live pups. Arrows, uteri containing fetuses (R, 4 fetuses; L, 3 fetuses). **d-f** Labor induction at 18 dpc does not rescue dystocia of *Setd3*$^{-/-}$ pregnant mice. **d,** Schematic of oxytocin treatment protocol. **e,** Quantification of births on d18 and d19 after oxytocin treatment from *Setd3*$^{+/+}$ (*n* = 7) and *Setd3*$^{-/-}$ (*n* = 5) mice. *, *p*-value = 0.042; **, *p*-value = 0.012. **f,** Quantification of fetuses *in utero* of mice from **e** (*Setd3*$^{+/+}$, *n* = 4; *Setd3*$^{-/-}$, *n* = 5). ***, *p*-value = < 0.001. **e,f,** *p*-values: unpaired two-tailed

student's *t* test. **a-b,e-f**; box and whisker parameters: center line, median; box limits, upper and lower quartiles; whiskers, maximum and minimum are indicated. **g-k,** Stimulus-induced contraction requires SETD3 and actin-H73me. **g,** Western blot analysis of primary uterine smooth muscle cells expressing CRISPR/Cas9 and control or SETD3-specific sgRNA. **h,** Representative images of a collagen contraction assay with cells from **g** ± oxytocin (OXT, 10 μM) or Endothelin-1 (Eth-1, 1 μM) after 24h. **i,** Quantification of **h.** Collagen disk area is measured for indicated conditions and normalized to the area without cells. ***** *p*-value = 0.019; **, *p*-value = 0.007. **j,** Western blot analysis of cells from **g** expressing SETD3$_{WT}$, catalytically dead SETD3$_{NHY}$, or a control vector. **k,** Quantification of contraction assays with reconstituted primary uterine cell lines as described in **i**. ***** *p*-value = 0.009; **, *p*-value = 0.006; ***, *p*-value = 0.001. **g-k,** Graphs indicate means with s.e.m. of experiments performed in biological triplicate. *p*-values from unpaired two-tailed student's *t*-test. All experiments were independently performed three times with similar results. For gel source data, see Supplementary Fig. 1.